CONFIDENTIAL

Copy No. 1
RM No. SL8K16

NACA

RESEARCH MEMORANDUM

for the

Bureau of Aeronautics, Department of the Navy

HIGH-SPEED WIND-TUNNEL INVESTIGATION OF THE LONGITUDINAL STABILITY AND CONTROL CHARACTERISTICS OF A 0.10-SCALE MODEL OF THE GRUMMAN XF9F-2 AIRPLANE

TED NO. NACA DE301

By

Edward C. Polhamus and Thomas J. King, Jr.

Langley Aeronautical Laboratory
Langley Field, Va.

16

CONFIDENTIAL

NATIONAL ADVISORY COMMITTEE FOR AERONAUTICS

RESEARCH MEMORANDUM

for the

Bureau of Aeronautics, Department of the Navy

HIGH-SPEED WIND-TUNNEL INVESTIGATION OF THE LONGITUDINAL STABILITY AND CONTROL CHARACTERISTICS OF A 0.10-SCALE MODEL OF THE GRUMMAN XF9F-2 AIRPLANE

TED NO. NACA DE301

By Edward C. Polhamus and Thomas J. King, Jr.

SUMMARY

An investigation was made in the Langley high-speed 7- by 10-foot tunnel to determine the high-speed longitudinal stability and control characteristics of a 0.10-scale model of the Grumman XF9F-2 airplane in the Mach number range from 0.40 to 0.85.

The results indicated that the lift and drag force breaks occurred at a Mach number of about 0.76. The aerodynamic-center position moved rearward after the force break and control position stability was present for all Mach numbers up to a Mach number of 0.85 except for a slight instability around a Mach number of 0.80.

INTRODUCTION

At the request of the Bureau of Aeronautics an investigation of the high-speed longitudinal stability and control characteristics of a 0.10-scale model of the Grumman XF9F-2 airplane was conducted in the Langley high-speed 7- by 10-foot tunnel.

This paper presents the results of the longitudinal stability and control investigation at Mach numbers ranging from 0.40 to 0.85. Pitch tests were conducted for various elevator and stabilizer settings and included tests to determine the effect of adding a horn balance to the elevator. The effect of wing-tip tanks on the longitudinal stability characteristics of the model was also investigated.

COEFFICIENTS AND SYMBOLS

The stability system of axes used for the presentation of the data, together with an indication of the positive forces, moments and angles, is presented in figure 1. Pertinent symbols are defined as follows:

C_L	lift coefficient (Lift/qS)
C_D	drag coefficient (Drag/qS)
C_m	pitching-moment coefficient measured about the 25-percent mean-geometric-chord position (Pitching-moment/qSc')
q	free-stream dynamic pressure, pounds per square foot $\left(\frac{\rho V^2}{2}\right)$
ρ	mass density of air, slugs per cubic foot
V	free-stream velocity, feet per second
S	wing area, square feet
c'	wing mean geometric chord (M.G.C.), feet
b	wing span, feet
M	Mach number (V/a)
a	velocity of sound, feet per second
R	Reynolds number $\left(\frac{\rho V c'}{\mu}\right)$
μ	absolute viscosity, pound-seconds per square foot
α	angle of attack of model, measured from the X-axis to the fuselage reference line, degrees
δ_e	elevator deflection with reference to stabilizer chord line, degrees
i_t	stabilizer setting with reference to fuselage reference line, degrees

$$C_{L_\alpha} = \frac{\partial C_L}{\partial \alpha}$$

$$C_{m_{\delta_e}} = \frac{\partial C_m}{\partial \delta_e}$$

$$C_{m_{i_t}} = \frac{\partial C_m}{\partial i_t}$$

$$C_{m_{C_L}} = \frac{\partial C_m}{\partial C_L}$$

APPARATUS AND METHODS

Tunnel and Model

The tests were conducted in the Langley high-speed 7- by 10-foot tunnel, which is a closed rectangular tunnel of the return-flow type with a contraction ratio of 15.7 to 1.

The 0.10-scale model was constructed at the David Taylor Model Basin, Carderock, Maryland. It was constructed entirely of steel. Details of the model as tested are presented in figures 2 and 3. The model was tested through a Mach number range of 0.40 to 0.85 at various angles of attack on the sting support shown in figure 4. Elevator and stabilizer effectiveness and the effect of the wing-tip tanks (see table I) were investigated throughout the Mach number and angle-of-attack ranges.

The variation of test Reynolds number with Mach number for average test conditions is presented in figure 5. The degree of turbulence of the tunnel is not known but is believed to be small because of the high contraction ratio. Experience has indicated that for a model of this size constriction effects should not invalidate the test results at corrected Mach numbers below about 0.91.

Support System

A sting support system was used to support the model in the tunnel and a photograph of the test setup is presented as figure 4. The sting extended from the rear of the fuselage to a vertical strut located behind the test section. This strut was mounted on the tunnel balance system and was shielded from the air stream by a streamline fairing. The tare forces and moments produced by the sting were determined by mounting the model on two wing stings, which were also attached to the vertical strut, and testing the model with and without the center sting. With the center sting in

[redacted]

place the duct flow was by-passed through a hole in the underside of the aft portion of the fuselage while without the center sting the flow was exhausted out of the rear of the fuselage. Therefore, the corrected data represent the condition with flow out of the rear of the fuselage. Angles of attack were changed by the use of interchangeable couplings in the stings aft of the model. The deflections of the support system under load were determined from static loading tests.

Corrections

The test results have been corrected for the tare forces and moments produced by the support system. The jet-boundary corrections were computed from the following equations, which were determined by the method of reference 1:

$$\alpha = \alpha_m + 0.26C_L$$

$$C_D = C_{D_m} + 0.0045C_L^2$$

$$C_m = C_{m_m} + 0.007C_L$$

where the subscript m indicates measured value.

The drag has been corrected for the buoyancy produced by the longitudinal static-pressure gradient in the tunnel, and the dynamic pressure and Mach number have been corrected for blocking by the model and its wake by the method of reference 2.

[redacted]

RESULTS AND DISCUSSION

Basic Data

The basic data for the various configurations tested are presented in the following table:

Type of test	Tip tanks	Elevator	Figure
Elevator effectiveness	On	Plain	6
Elevator effectiveness	Off	Plain	7
Elevator effectiveness	On	Horn balanced	8
Stabilizer	On	Plain	9

General Aerodynamic Characteristics

A summary of some of the more important aerodynamic parameters as evaluated from the basic data is presented in figures 10 and 11.

Lift and drag.- The lift-curve slope (fig. 10) increases with Mach number up to a Mach number of about 0.76, above which there is a rapid reduction. The end-plate effect of the wing-tip tanks increased the lift-curve slope by about 15 percent at a Mach number of 0.40 and by about 20 percent at the force break Mach number of 0.76. Above the Mach number for lift force break the effect of the tip tanks rapidly diminished. Low-speed wind-tunnel tests of a similar configuration (reference 3) indicate a tank effect of the same order of magnitude as that obtained at the lowest Mach number in the present investigation.

The drag at zero lift (fig. 10) decreases slightly with increasing Mach number up to the drag force break Mach number of about 0.76. This effect has been observed on other models and has been attributed to the increase in Reynolds number with increasing Mach number. Above a Mach number of 0.76 there is a rather rapid drag rise due to the onset of compressibility effects. The wing-tip tanks added a constant drag-coefficient increment of about 0.002 up to a Mach number of about 0.76. The rate of increase of drag coefficient with Mach number above the drag break Mach number was somewhat greater with the wing-tip tanks on than with them off.

[redacted]

The maximum value of the lift-drag ratio (fig. 10) is fairly constant up to a Mach number of about 0.75, above which it decreases. Except at the low Mach numbers the maximum lift-drag ratio is greater for the tip-tanks-off condition. The effect of the wing-tip tanks on the variation of the lift-drag ratio with lift coefficient for several Mach numbers is presented in figure 11. Only at the lower Mach numbers in the high lift range where the induced drag is important is there an increase in the lift-drag ratio due to the end-plate effect of the wing-tip tanks.

Control effectiveness.- The elevator and stabilizer effectiveness increased slightly with Mach number up to 0.76 and 0.80, respectively, above which they both decreased rapidly. The horn balance (fig. 3) had a negligible effect on the elevator effectiveness (figs. 6 and 8) as did the wing-tip tanks (fig. 7). The ratio of elevator to stabilizer effectiveness at a Mach number of 0.40 is about 0.76. Although this ratio seems high when compared with an estimated value of flap lift effectiveness of about 0.62 (reference 4), it is in good agreement with low-speed wind-tunnel tests of a larger scale model of the same airplane (references 5 and 6).

Aerodynamic center.- The rate of change of pitching-moment coefficient with lift coefficient at a constant Mach number $C_{m_{C_L}}$ (fig. 10) is a measure of the aerodynamic-center location relative to the assumed center-of-gravity position in percent of the mean geometric chord. The aerodynamic center is seen to move forward from about 10 percent behind the center of gravity at a Mach number of 0.40 to about 8 percent at a Mach number of 0.76 and then moves rapidly rearward. The wing-tip tanks shifted the aerodynamic center forward by about 1 percent throughout the Mach number range.

Estimated Flight Characteristics

Performance.- The variation of the lift coefficient required for level flight with Mach number for various wing loadings and altitudes is presented in figure 12. Also presented are the lift-drag ratios corresponding to the level-flight lift coefficients. The variation of these lift-drag ratios illustrates the advantage of flying at the higher altitude.

Static longitudinal stability.- The variation of the elevator position with Mach number is presented in figure 12 for various wing loadings and altitudes. Control position stability is present throughout the Mach number range except for a small region around a Mach number of 0.80. However, the trim changes associated with this instability are very slight.

[redacted]

Maneuvering stability.- The response of an airplane to gusts and rapid control deflections is governed by the location of the aerodynamic center and the damping of the horizontal tail. Inasmuch as the damping of the tail will be stabilizing and the aerodynamic-center position (fig. 10) is never less than 8 percent of the mean geometric chord behind the assumed center-of-gravity position, maneuvering stability will be present throughout the Mach number range tested.

CONCLUSIONS

Based on high-speed wind-tunnel tests of a 0.10-scale model of the Grumman XF9F-2 airplane in the Mach number range from 0.40 to 0.85, the following conclusions have been reached:

1. Lift and drag force breaks occurred at a Mach number of about 0.76.

2. The position of the aerodynamic center moved forward only about 2 percent of the mean geometric chord up to the force break and moved rearward rapidly after the force break.

3. Control position stability was present throughout the Mach number range except for a small region around a Mach number of 0.80. However, the trim changes associated with this instability are very slight.

4. Wing-tip tanks had minor effects on the stability characteristics but decreased the lift-drag ratio at the higher Mach numbers.

[redacted]

5. The horn balance had a negligible effect on the elevator effectiveness.

Langley Aeronautical Laboratory
National Advisory Committee for Aeronautics
Langley Field, Va.

Edward C Polhamus

Edward C. Polhamus
Aeronautical Research Scientist

Thomas J. King, Jr.

Thomas J. King, Jr.
Aeronautical Research Scientist

Approved: Thomas A. Harris

Thomas A. Harris
Chief of Stability Research Division

bpe

REFERENCES

1. Gillis, Clarence L., Polhamus, Edward C., and Gray, Joseph L., Jr.: Charts for Determining Jet-Boundary Corrections for Complete Models in 7- by 10-Foot Closed Rectangular Wind Tunnels. NACA ARR No. L5G31, 1945.

2. Herriot, John G.: Blockage Corrections for Three-Dimensional-Flow Closed-Throat Wind Tunnels, with Consideration of the Effect of Compressibility. NACA RM No. A7B28, 1947.

3. Tucker, Warren A., and Goodson, Kenneth W.: Tests of a 1/5-Scale Model of the Republic XP-84 Airplane (Army Project MX-578) in the Langley 300 MPH 7- by 10-Foot Tunnel. NACA MR No. L6F25, Army Air Forces, 1946.

4. Sears, Richard I.: Wind-Tunnel Data on the Aerodynamic Characteristics of Airplane Control Surfaces. NACA ACR No. 3L08, 1943.

5. Shuman, William H., and Watriss, Frederic W.: Wind Tunnel Tests on Grumman Aircraft Engineering Corporation Design 79-D, Fourth Series. M.I.T. Wind Tunnel Rep. No. 762, Feb. 1947.

6. Tamburello, V., and Beek, Charles R.: Wind-Tunnel Tests of a 1/5-Scale Powered Model of the XF9F-2 Airplane. Part I - Longitudinal Characteristics, Stabilizer Tests - TED No. TMB 301. Rep. C-131 Aero 758, David Taylor Model Basin, July 1948.

TABLE I.- ORDINATES OF WING-TIP TANKS

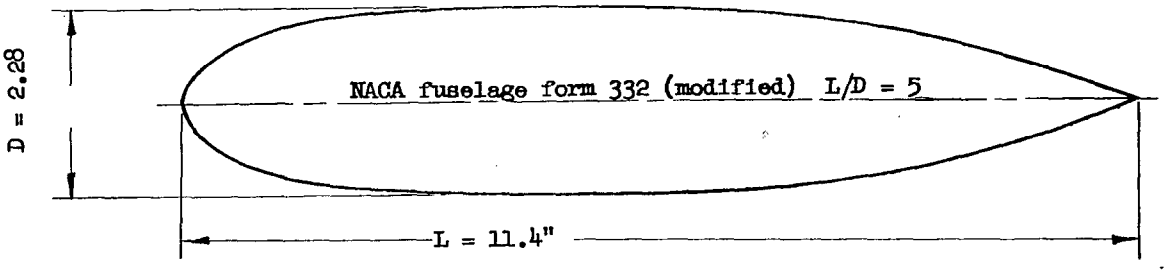

Station (percent length)	Ordinate (percent length)
0	0
.80	2.667
1.69	3.825
2.81	4.865
3.92	5.670
6.16	6.865
8.33	7.667
10.63	8.375
15.00	9.133
19.57	9.620
24.00	9.800
28.50	9.925
34.33	9.987
39.23	10.000
46.37	9.973
50.67	9.867
55.31	9.760
59.67	9.507
64.25	9.170
68.33	8.733
73.19	7.985
77.66	7.070
82.09	5.800
86.59	4.400
88.83	3.653
91.06	2.953
100.00	0
Nose radius = 4.00	

NACA

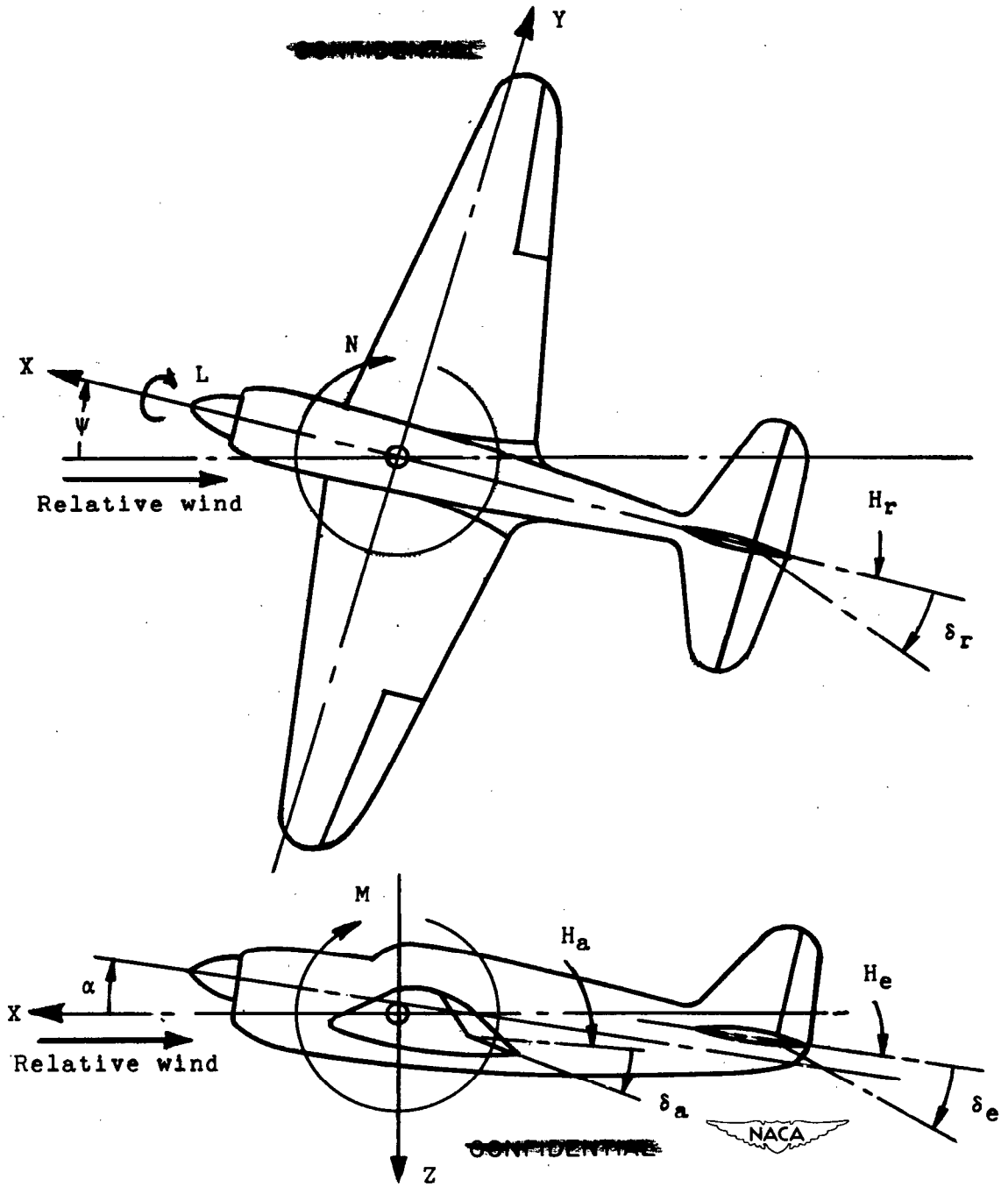

Figure 1.– System of axes and control-surface hinge moments and deflections. Positive values of forces, moments, and angles are indicated by arrows. Positive values of tab hinge moments and deflections are in the same directions as the positive values for the control surfaces to which the tabs are attached.

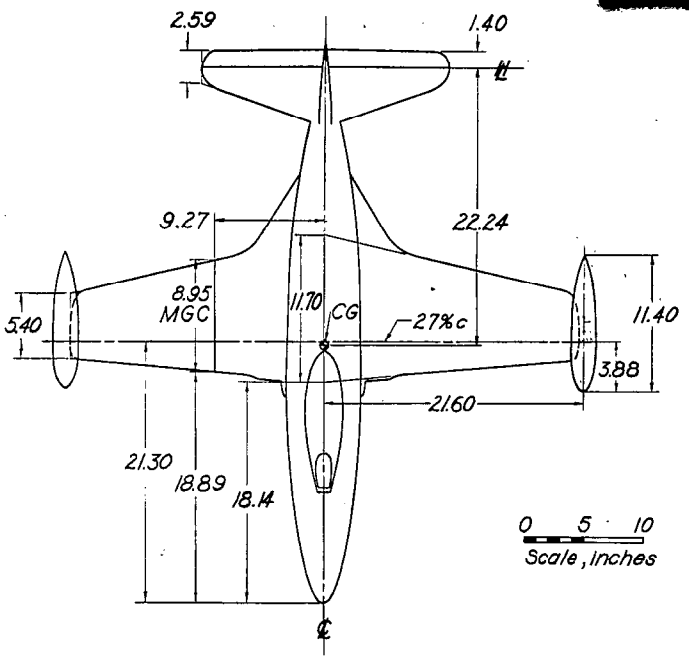

TABULATED DATA

Wing		
Section		NACA 64_1A012
Incidence		0°
Taper ratio		0.46
Aspect ratio		4.97
Area		2.50.0 sq ft
Mean Geometric Chord		0.746 ft
Horizontal tail		
Section	Tip	NACA 64A010
	Root	NACA 64_1A012
Taper ratio		0.417
Aspect ratio		4.71
Area		0.626 sq ft

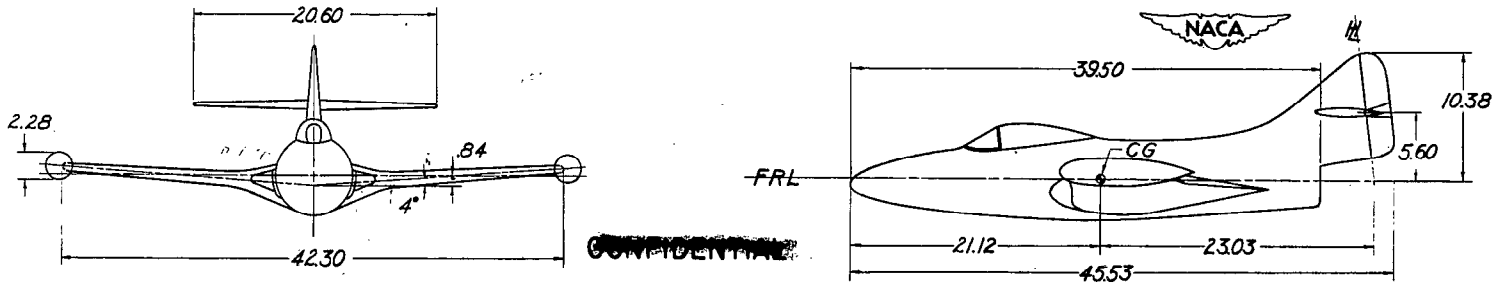

CONFIDENTIAL

Figure 2.- General arrangement of 0.10-scale model of Grumman XF9F-2 airplane.

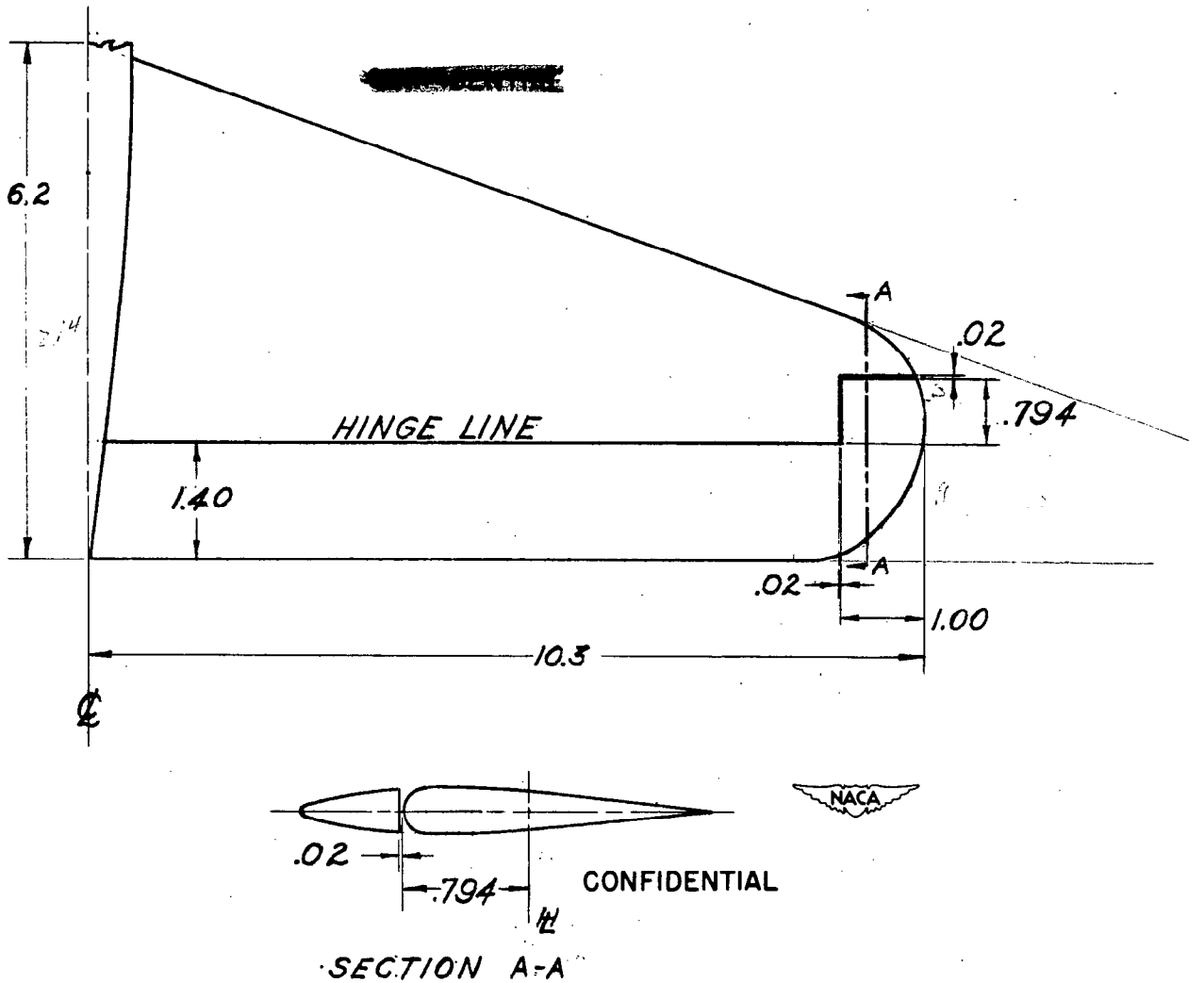

Figure 3.- Drawing of the stabilizer and horn-balanced elevator of the 0.10-scale model of the XF9F-2 airplane.

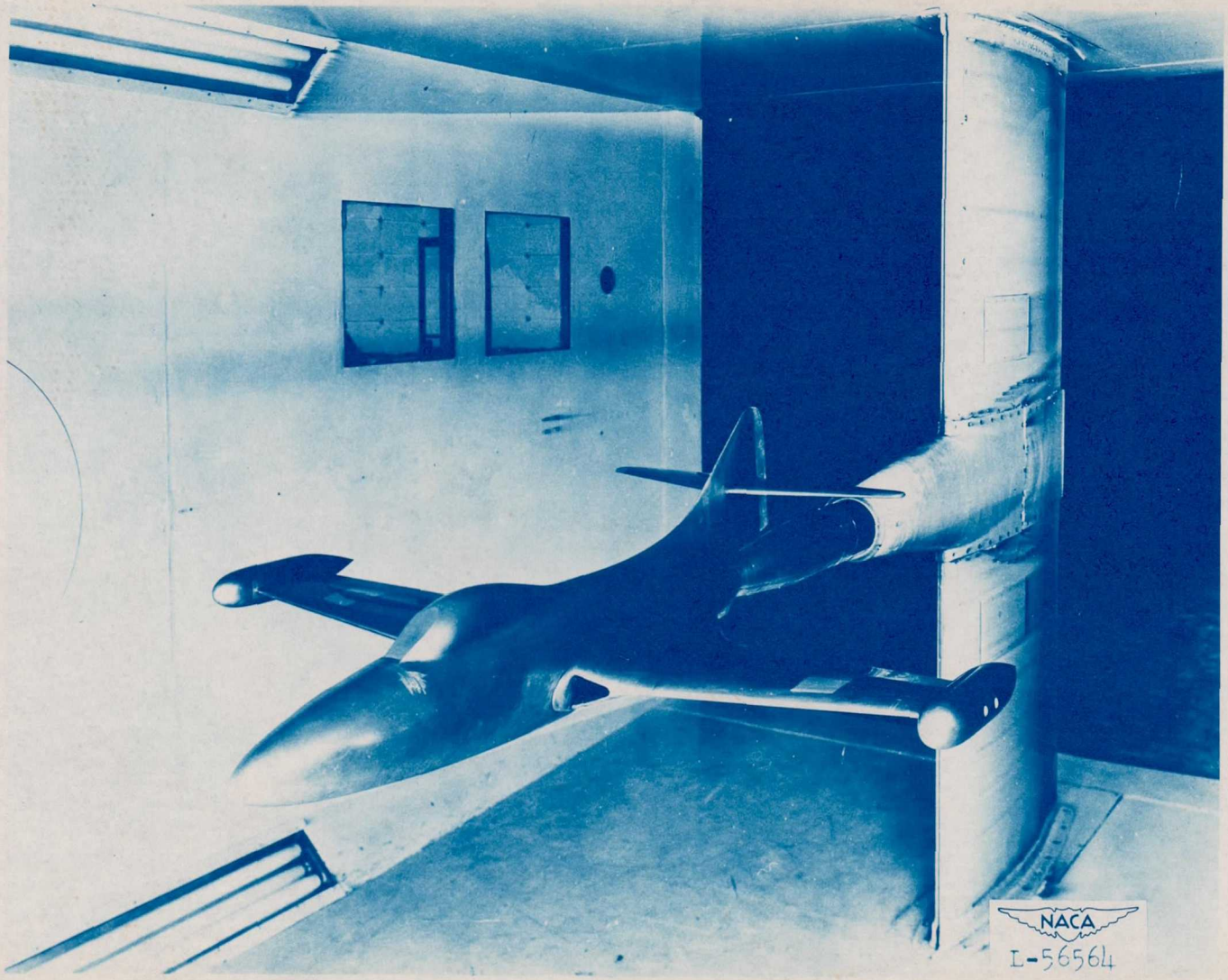

Figure 4.- The 0.10-scale model of the XF9F-2 airplane mounted on the sting support.

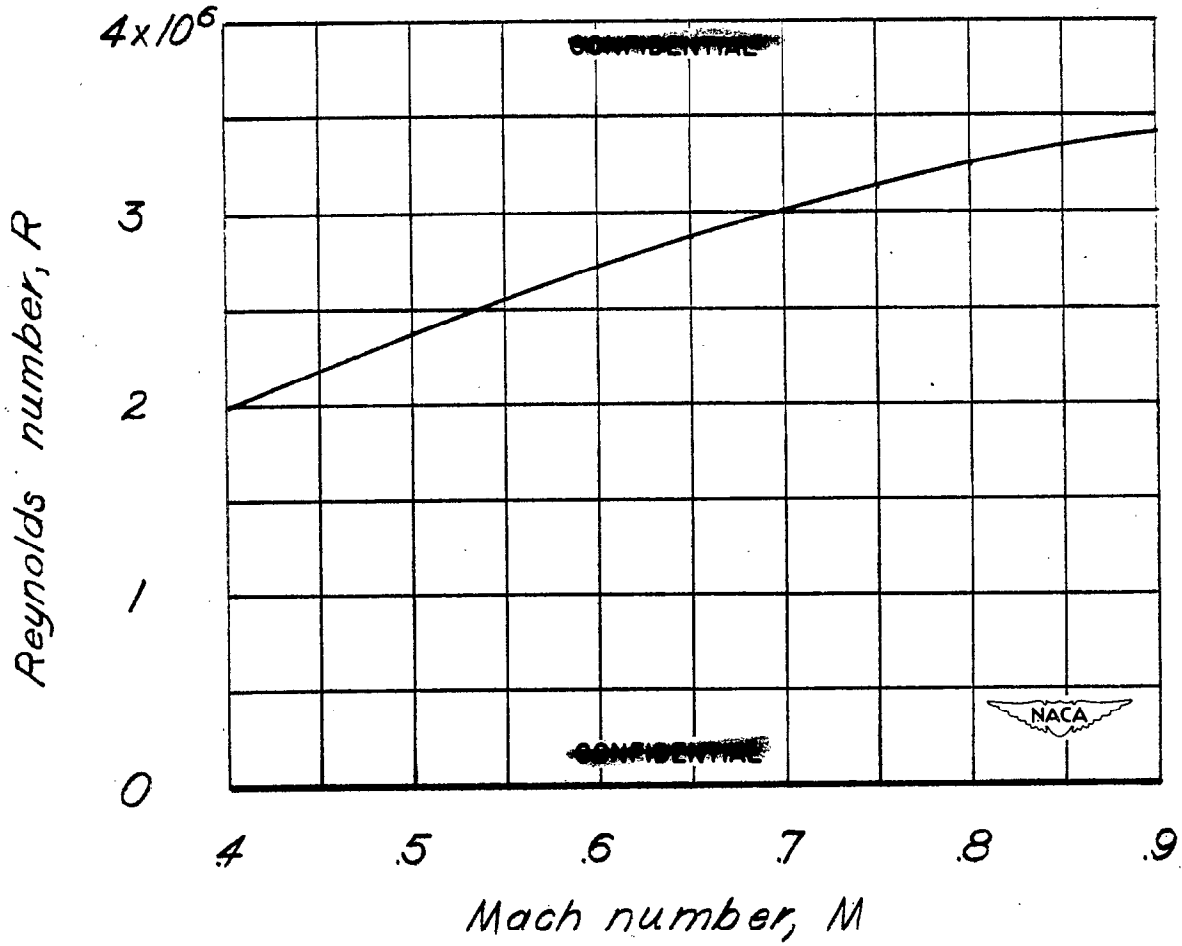

Figure 5.- Variation of test Reynolds number with Mach number for the 0.10-scale model of the XF9F-2 airplane.

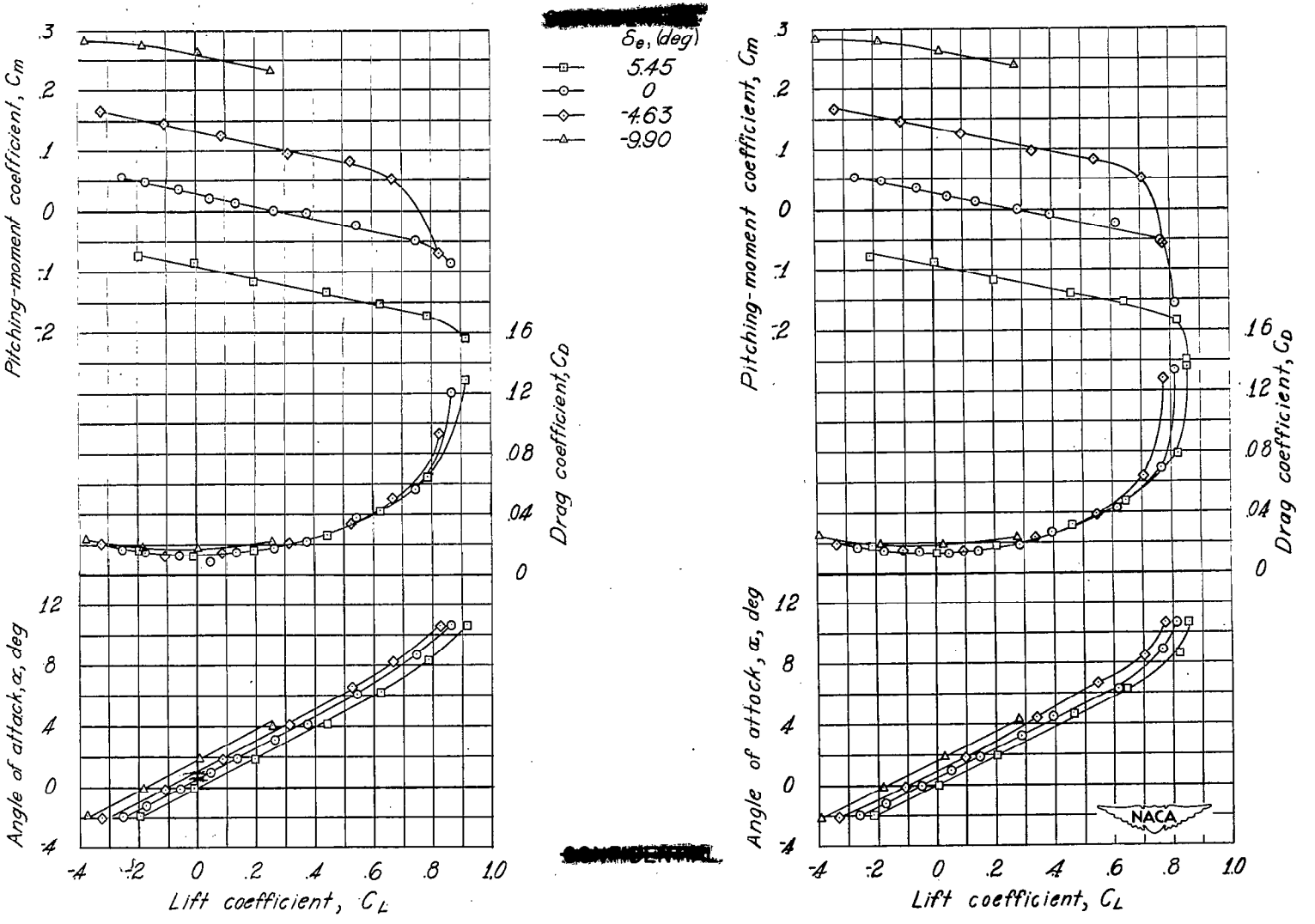

(a) M = 0.400.

(b) M = 0.500.

Figure 6.– Effect of elevator deflection on the aerodynamic characteristics in pitch of the 0.10–scale model of the XF9F–2 airplane. Plain elevator; tanks on; $i_t = 0°$.

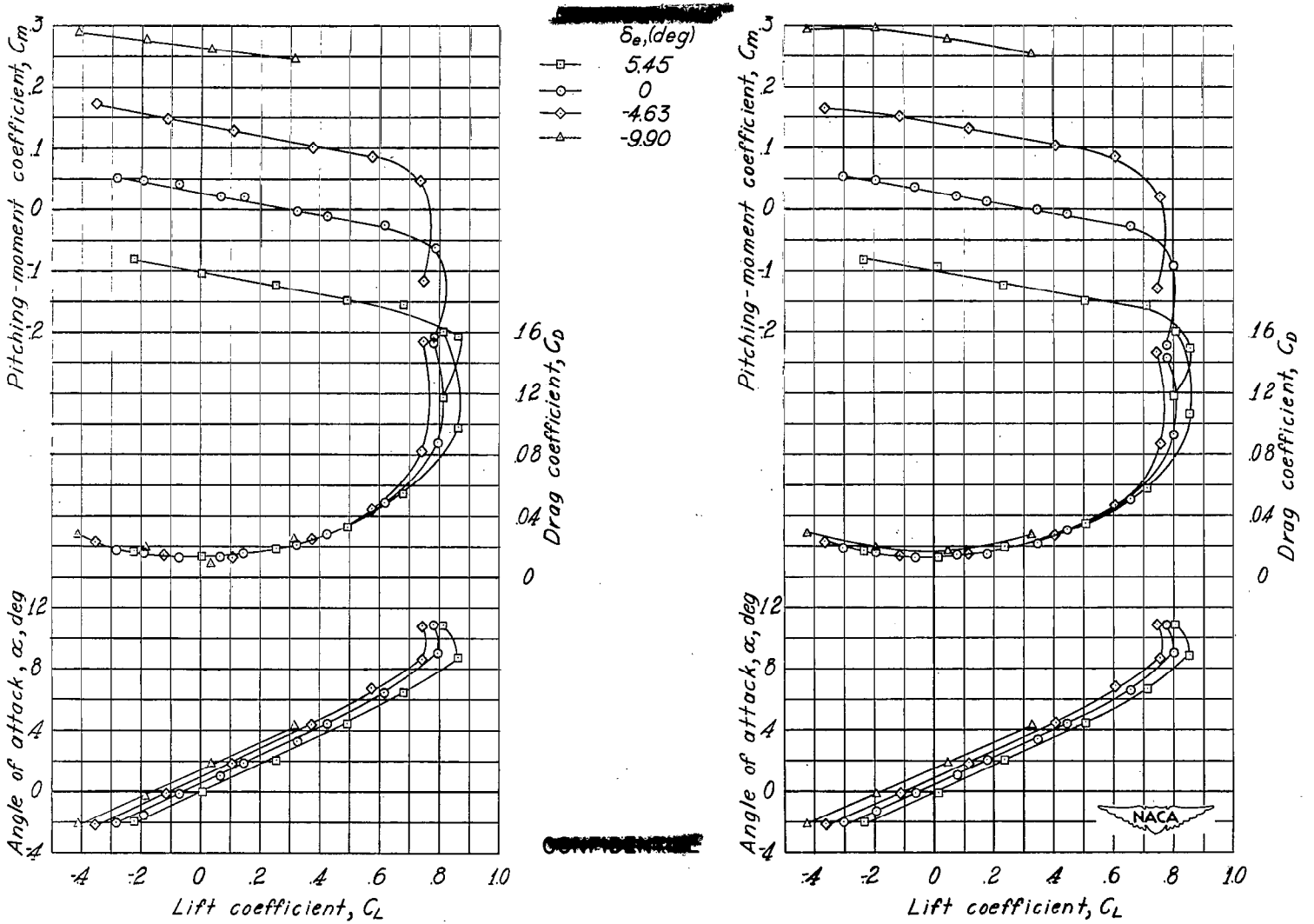

(c) M = 0.600.

(d) M = 0.650.

Figure 6.– Continued.

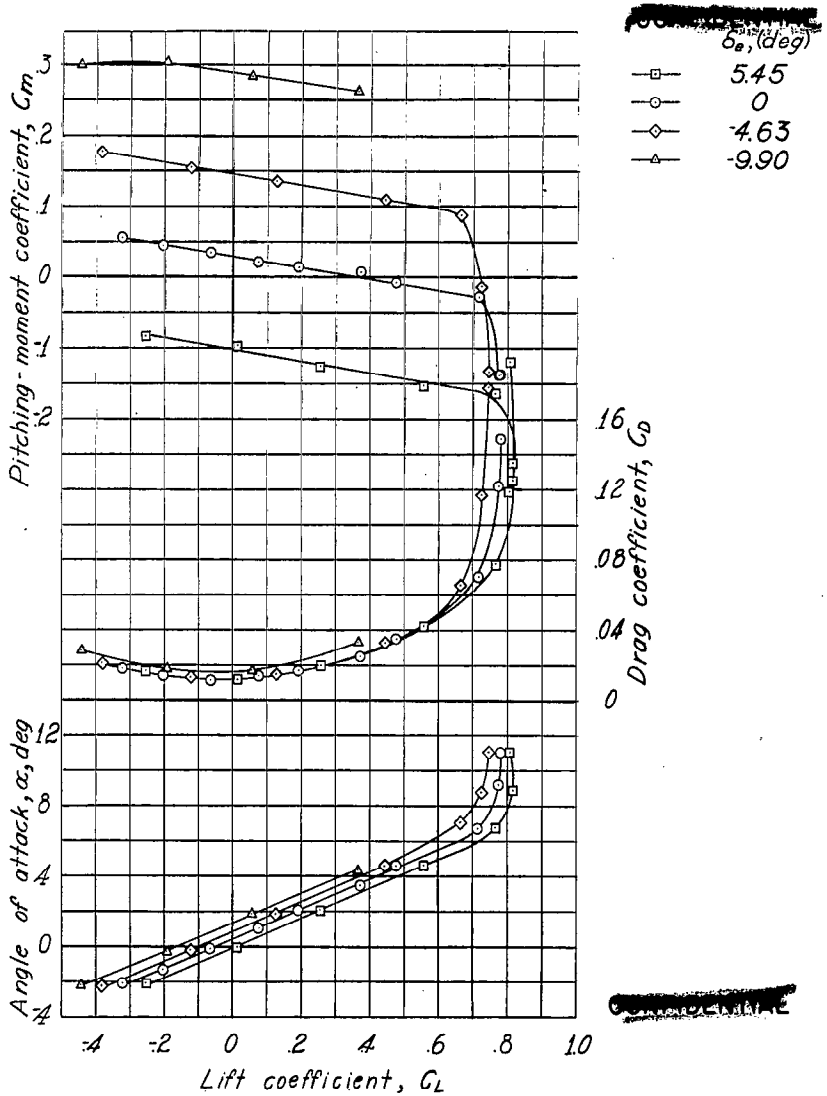

(e) M = 0.700.

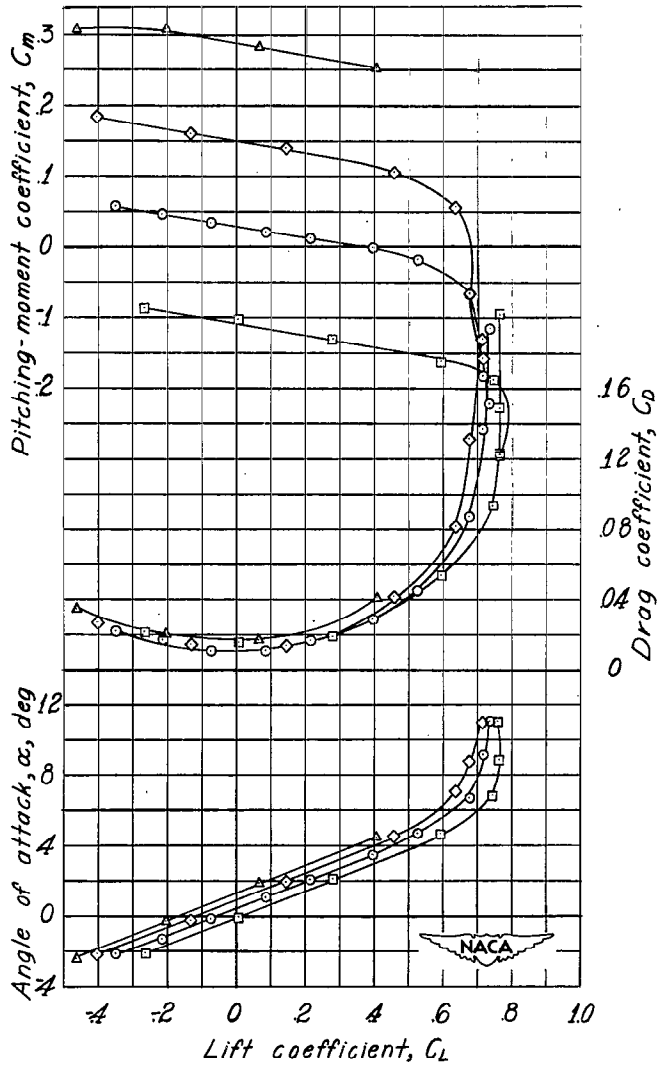

(f) M = 0.750.

Figure 6.– Continued.

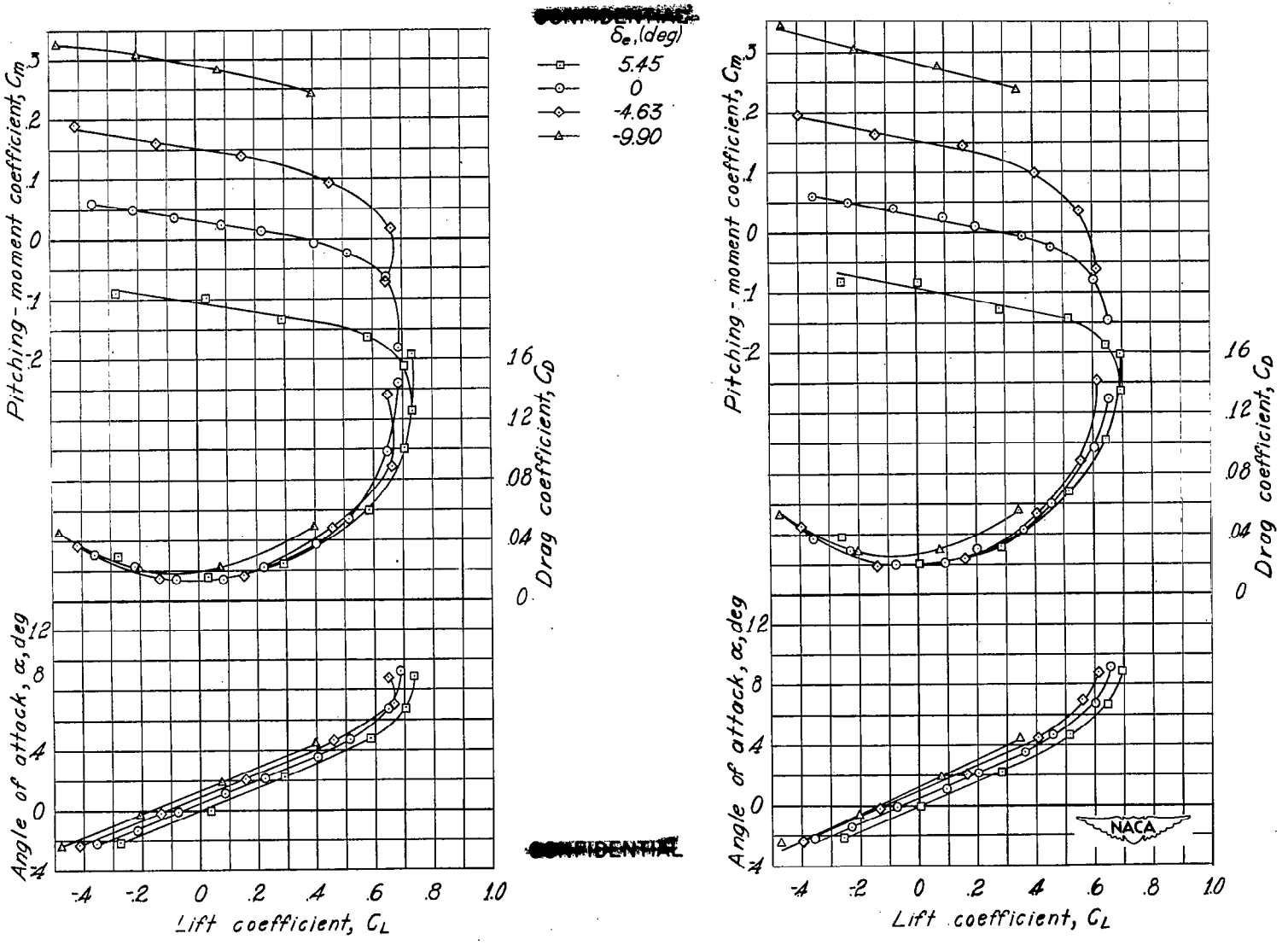

(g) M = 0.775.

(h) M = 0.800.

Figure 6.– Continued.

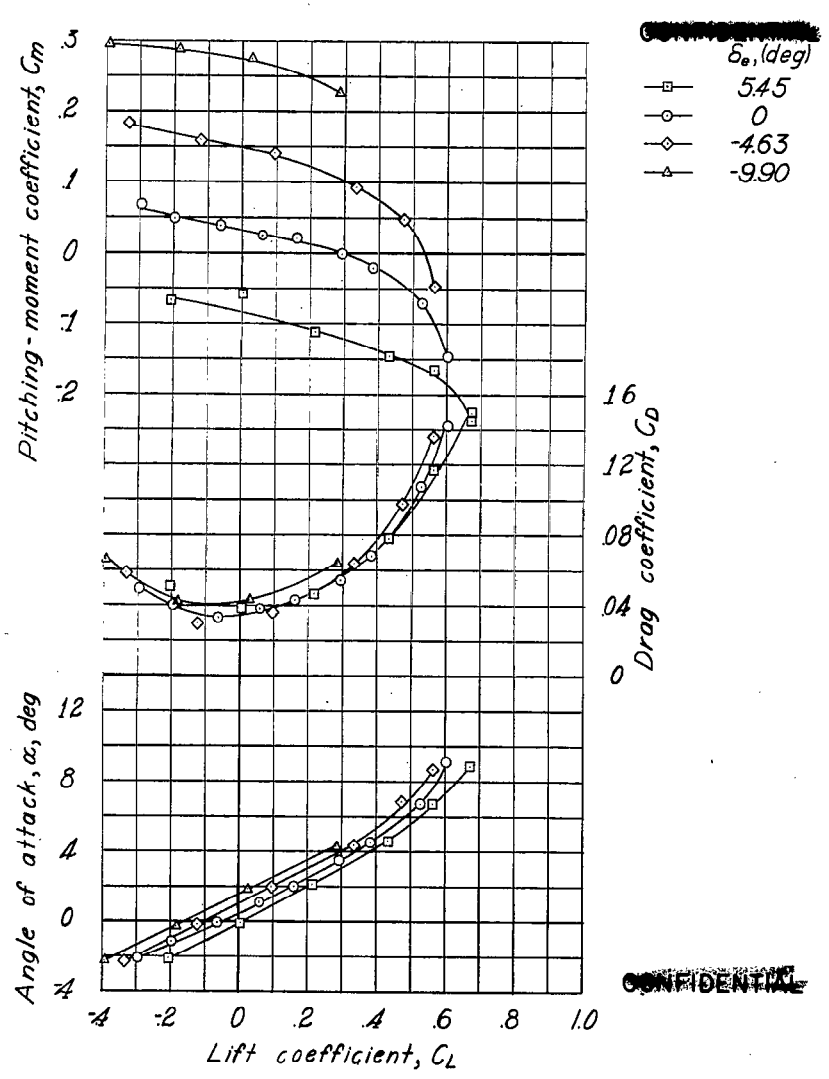

(i) M = 0.825.

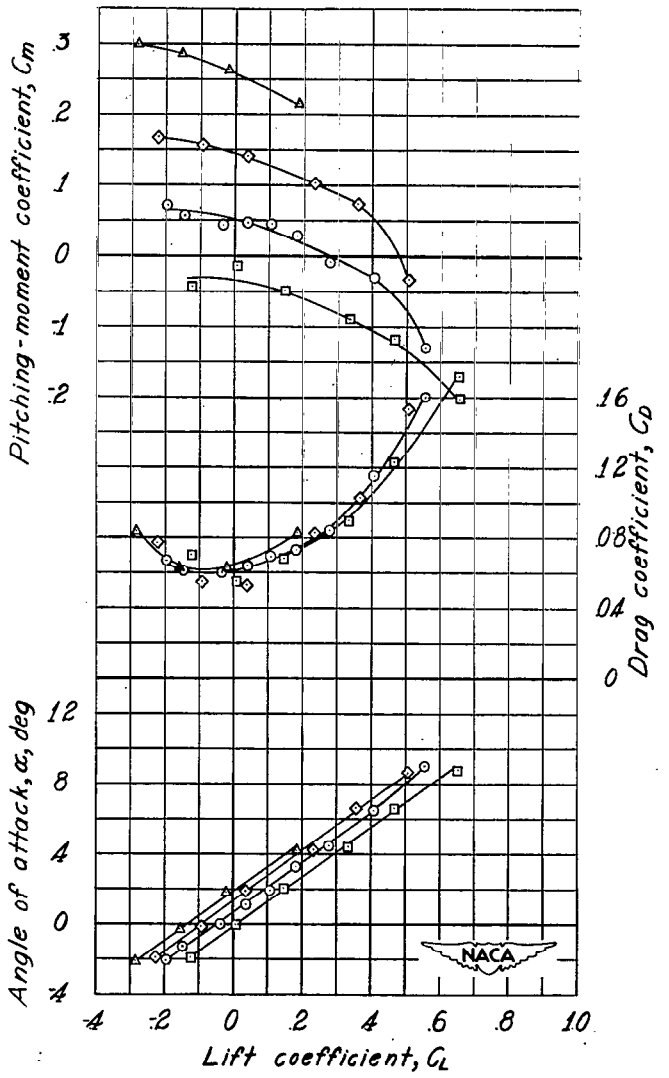

(j) M = 0.850.

Figure 6.– Concluded.

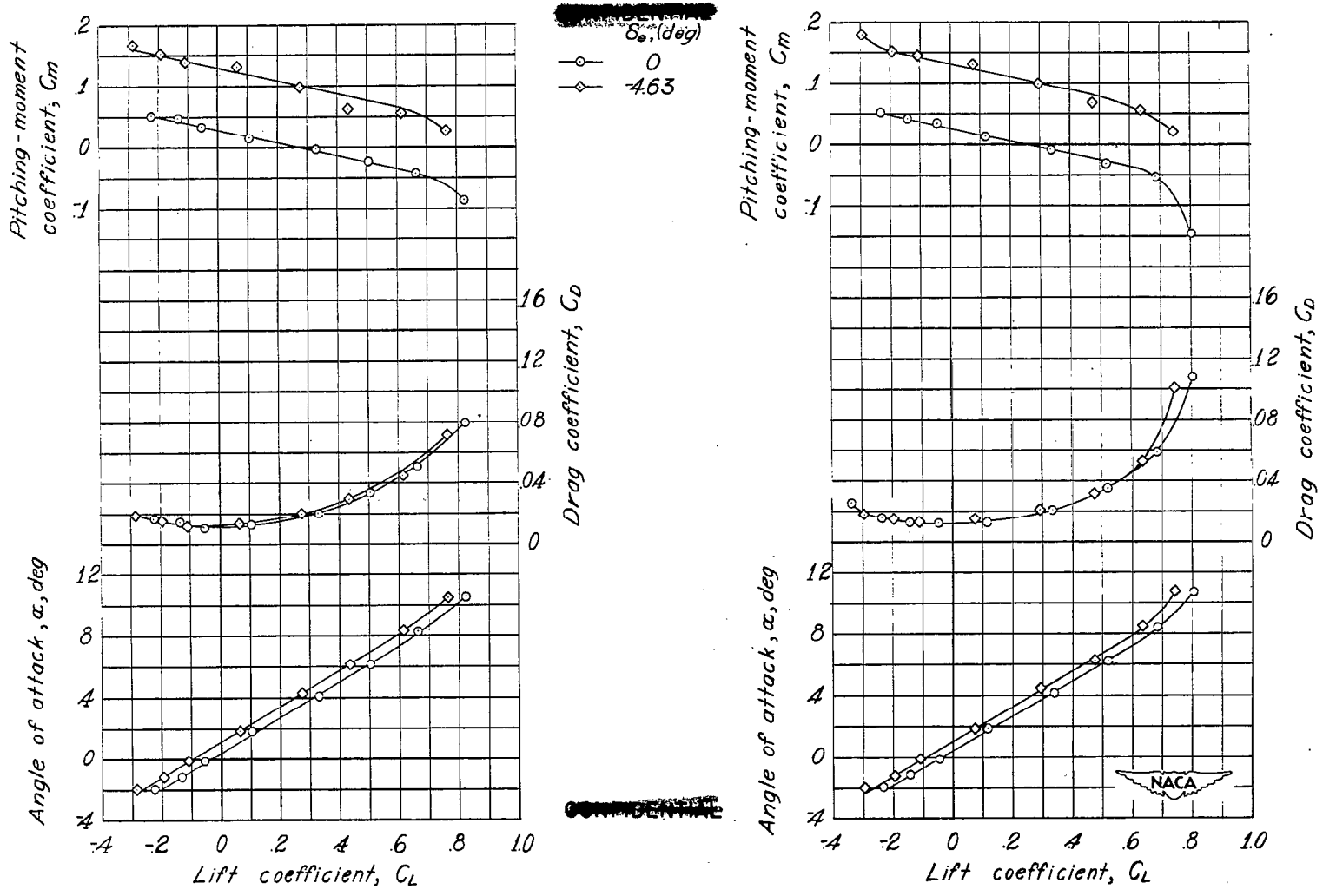

(a) M = 0.400.

(b) M = 0.500.

Figure 7.– Effect of elevator deflection on the aerodynamic characteristics in pitch of the 0.10–scale model of the XF9F–2 airplane. Plain elevator; tanks off; $i_t = 0^\circ$.

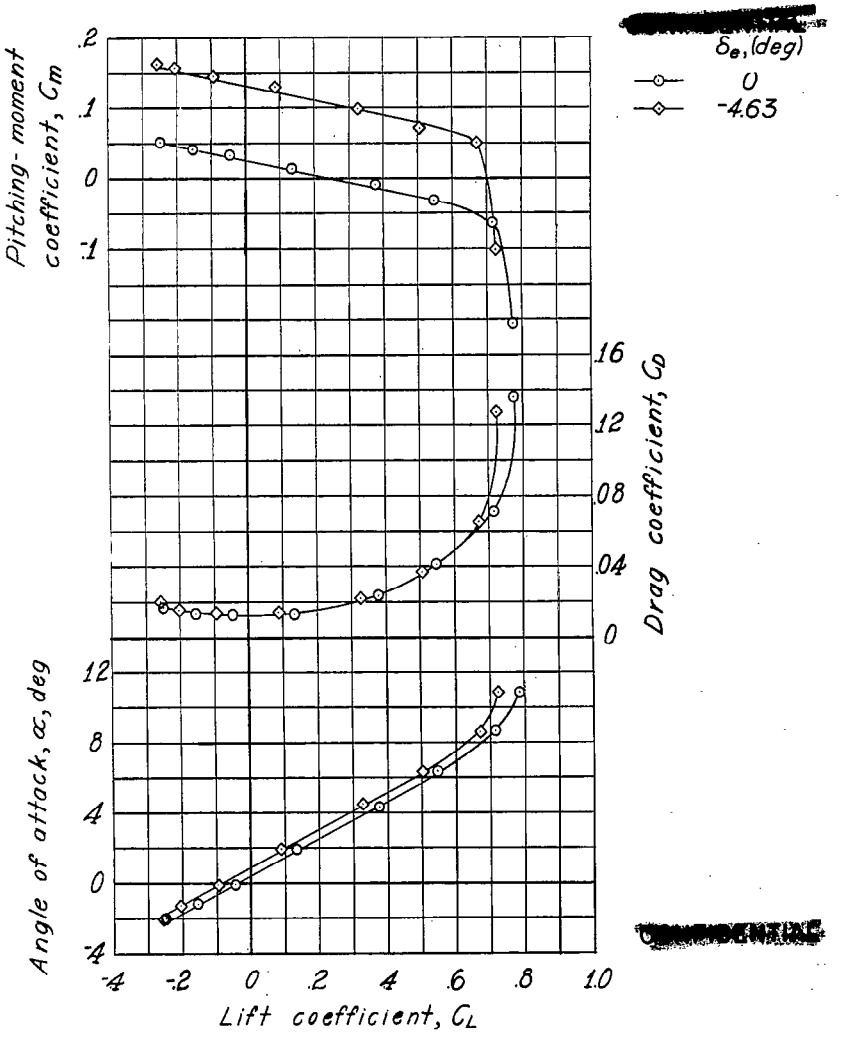

(c) M = 0.600.

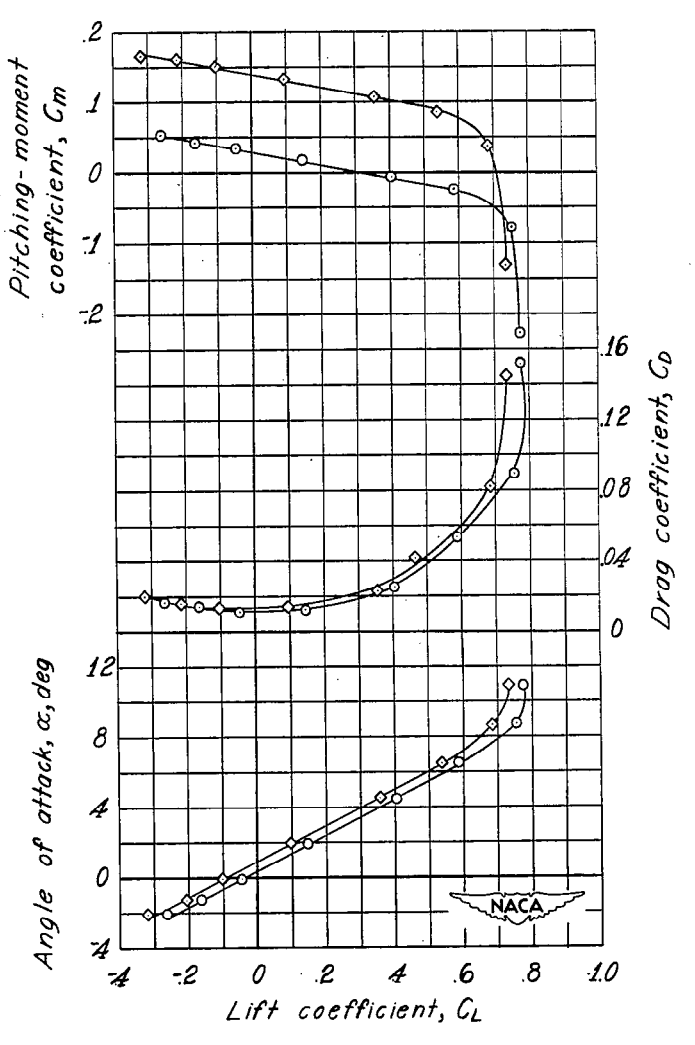

(d) M = 0.650.

Figure 7.– Continued.

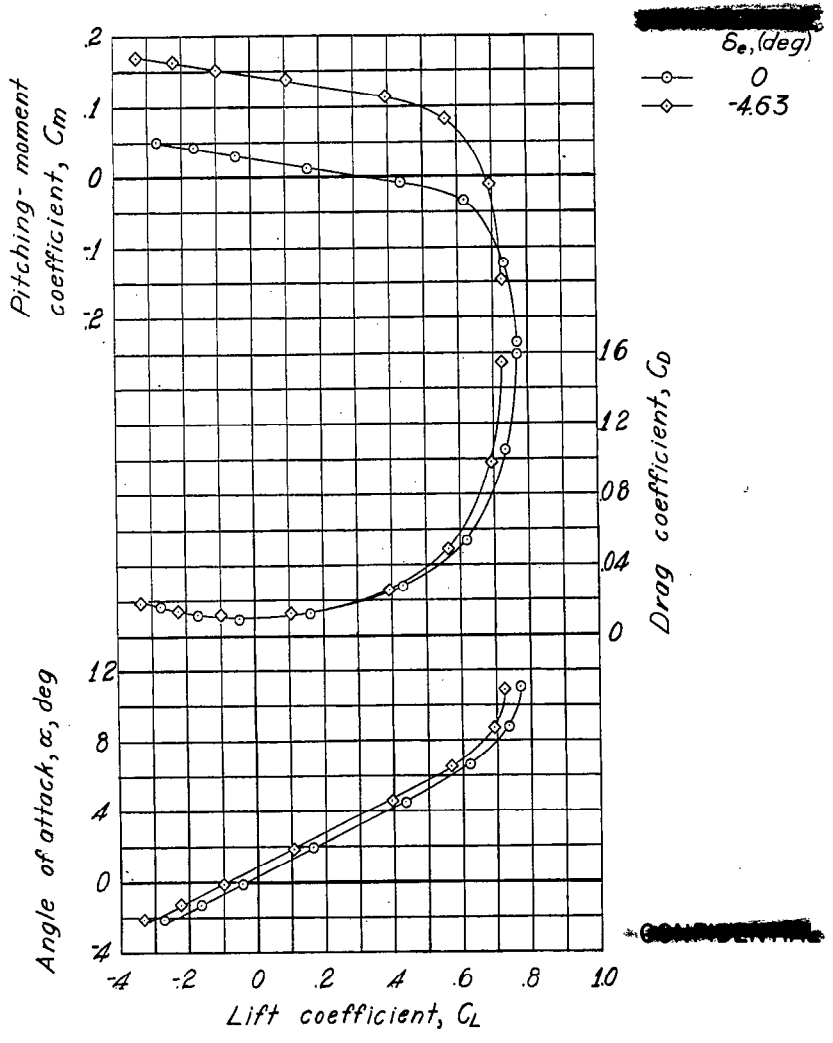

(e) M = 0.700.

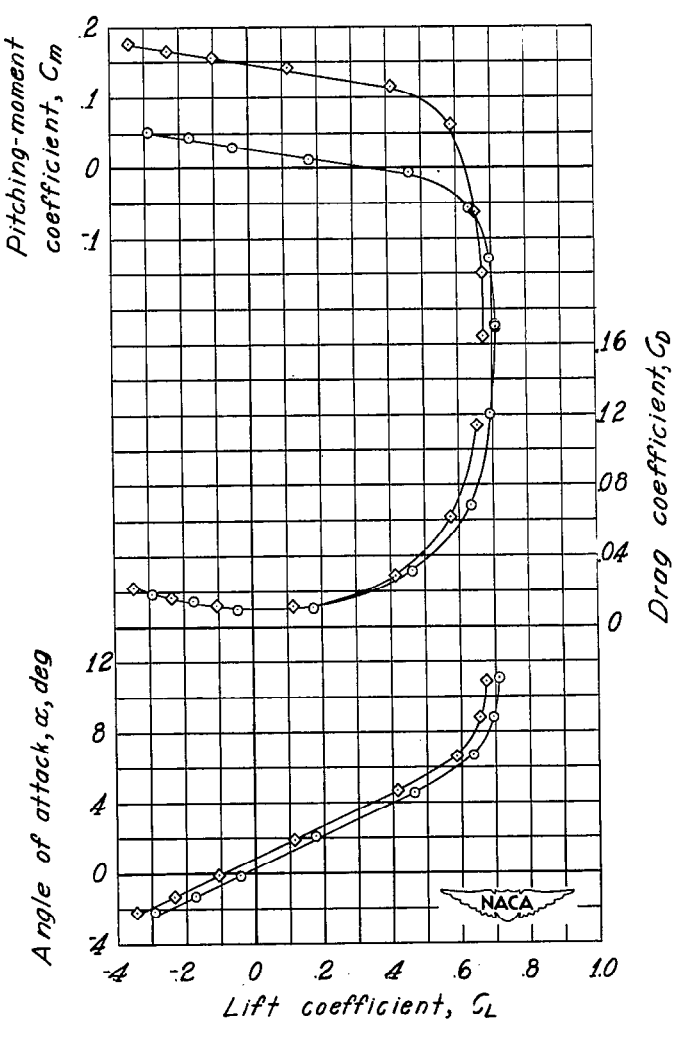

(f) M = 0.750.

Figure 7.- Continued.

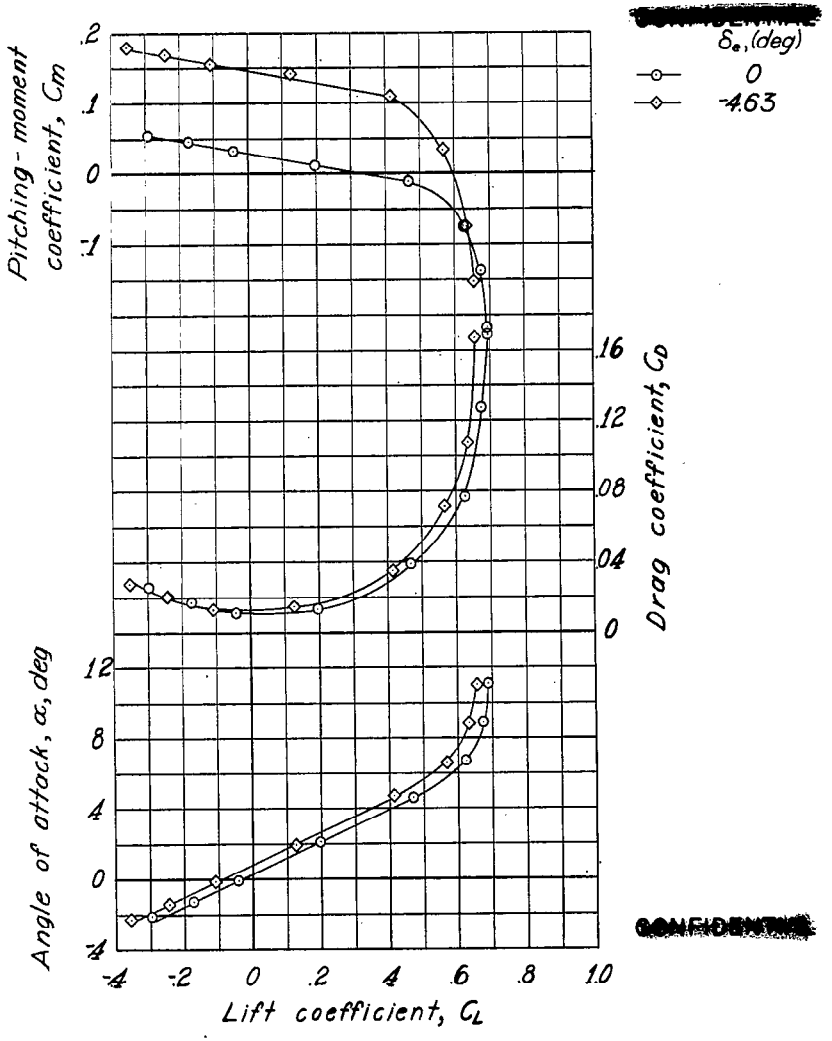

(g) M = 0.775.

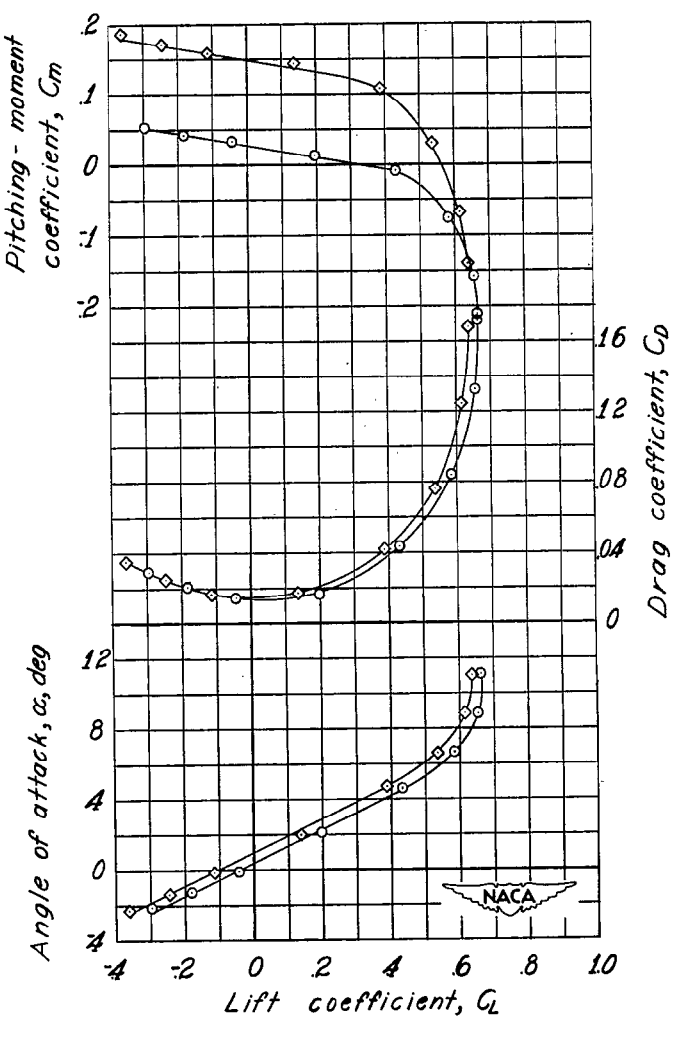

(h) M = 0.800.

Figure 7.- Continued.

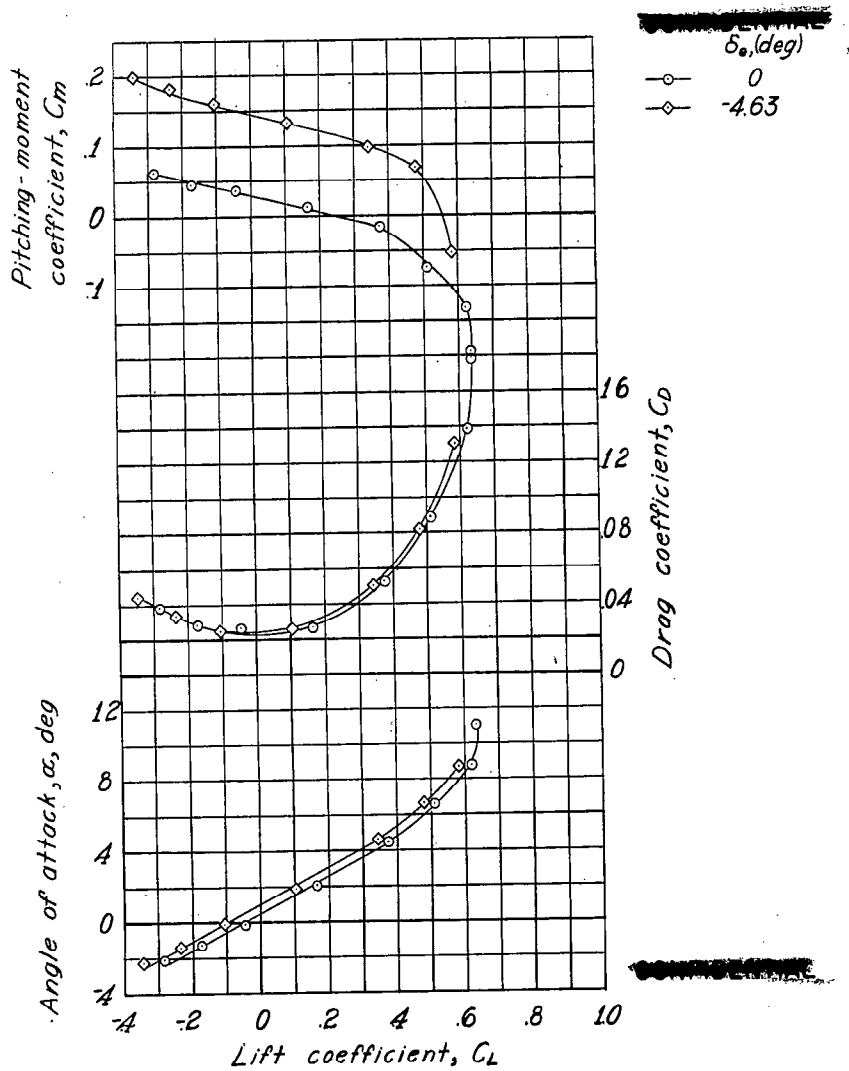

(i) M = 0.825.

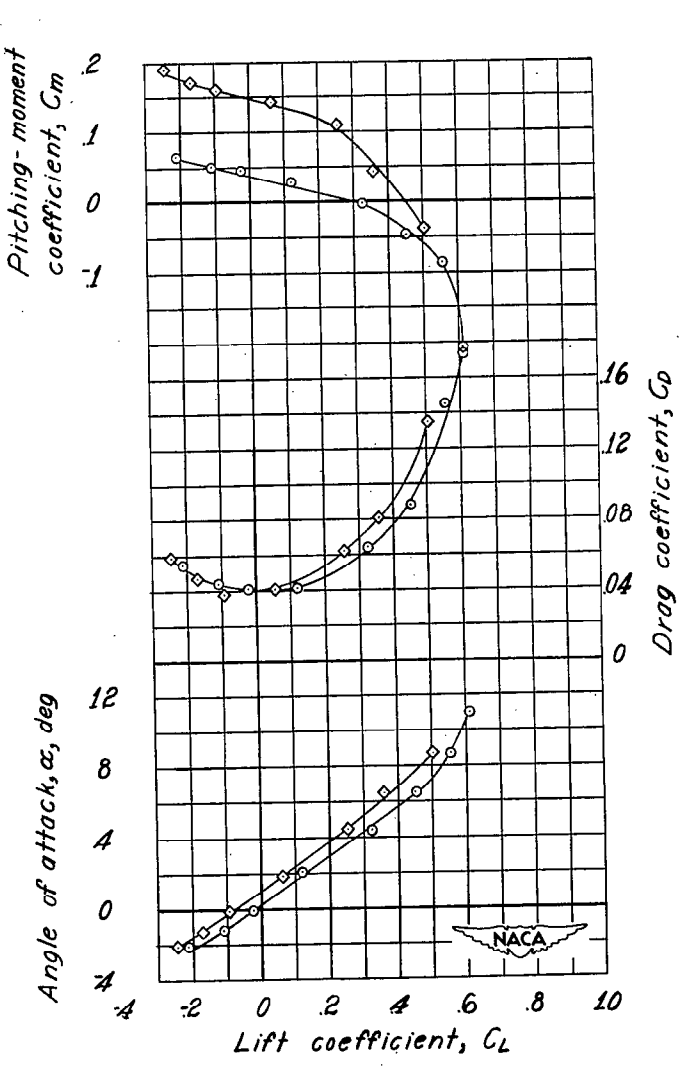

(j) M = 0.850.

Figure 7.- Concluded.

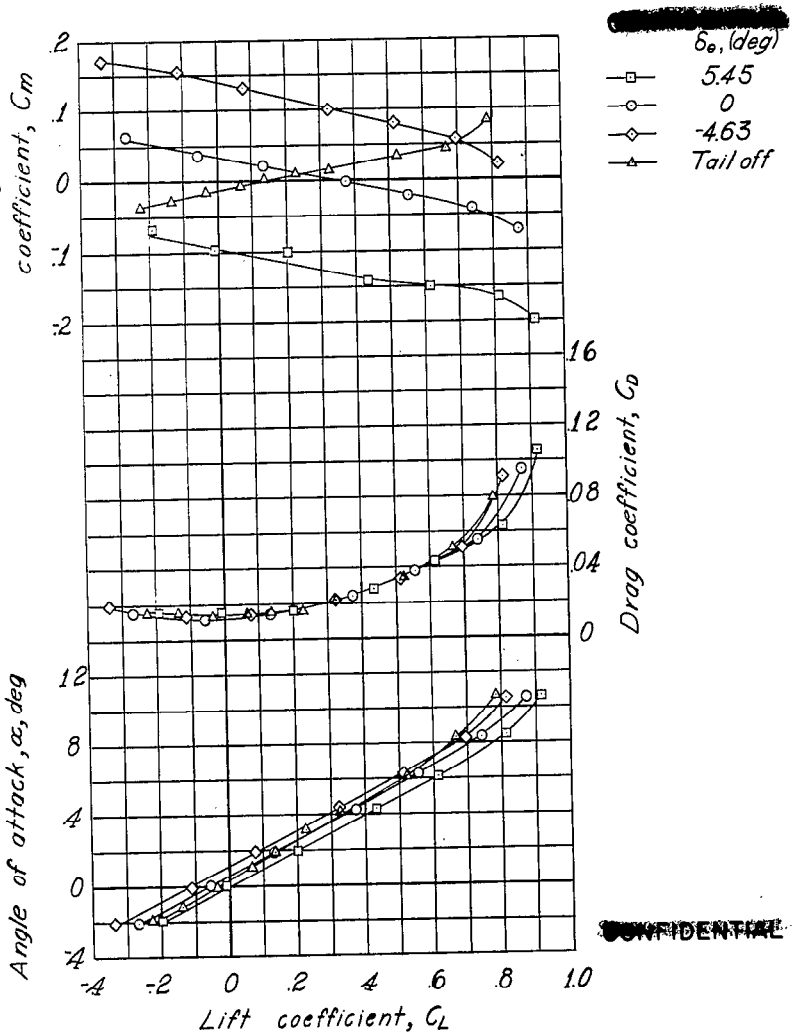

(a) M = 0.400.

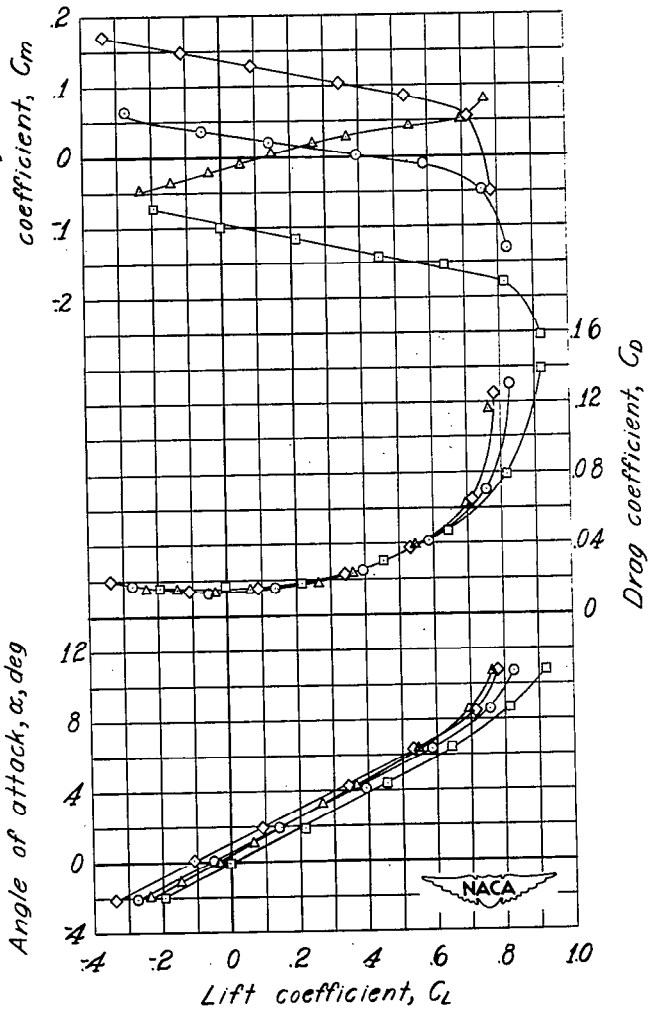

(b) M = 0.500.

Figure 8.– Effect of elevator deflection on the aerodynamic characteristics in pitch of the 0.10–scale model of the XF9F–2 airplane. Horn–balanced elevator; tanks on; $i_t = 0^o$.

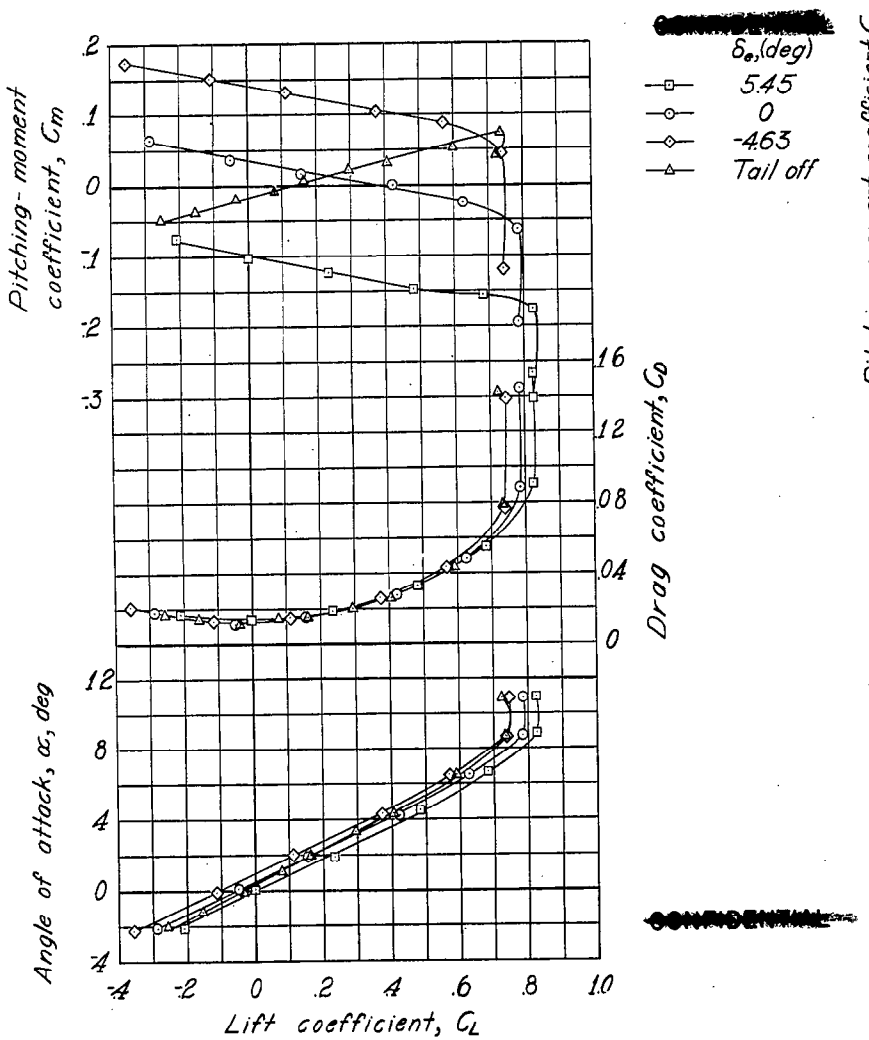

(c) M = 0.600.

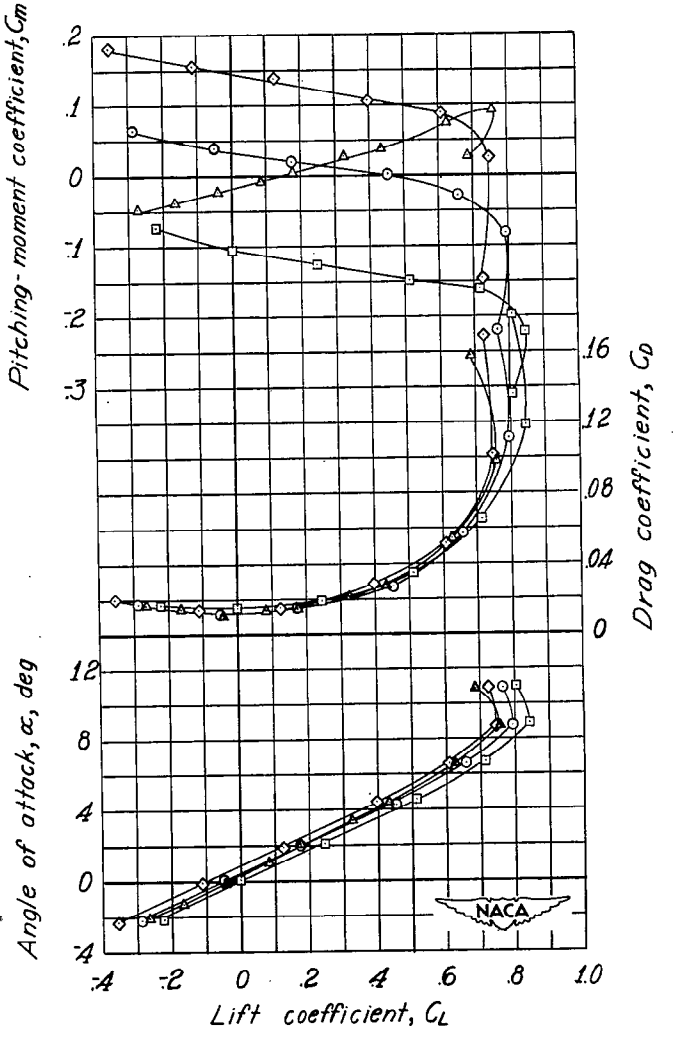

(d) M = 0.650.

Figure 8.- Continued.

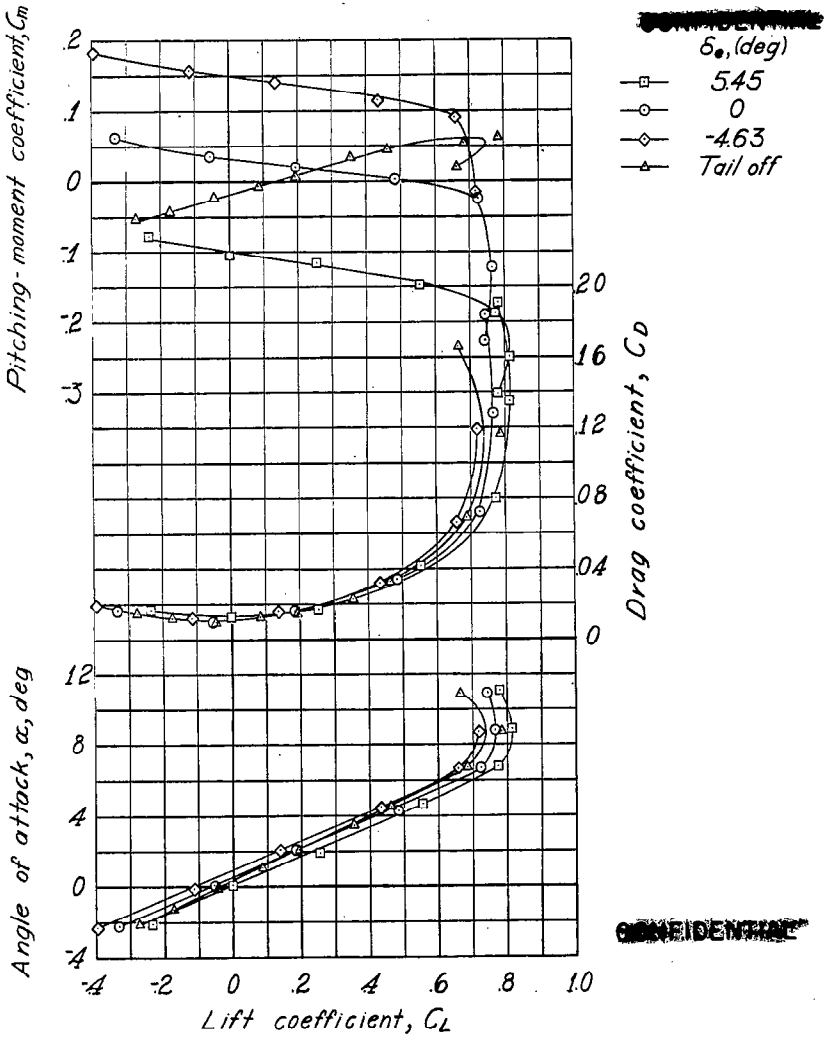

(e) M = 0.700.

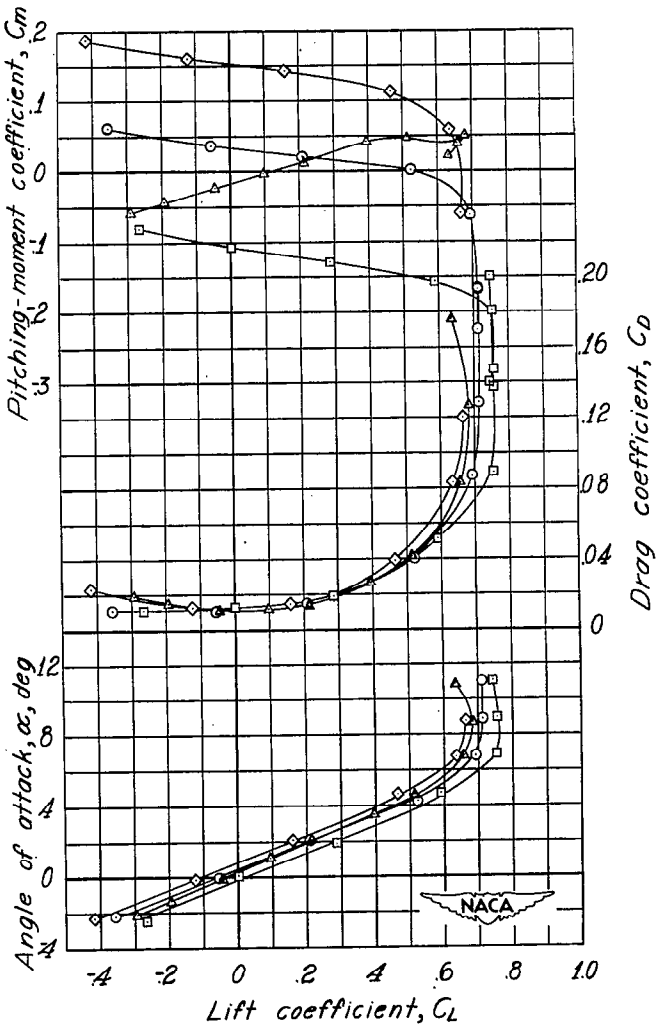

(f) M = 0.750.

Figure 8.– Continued.

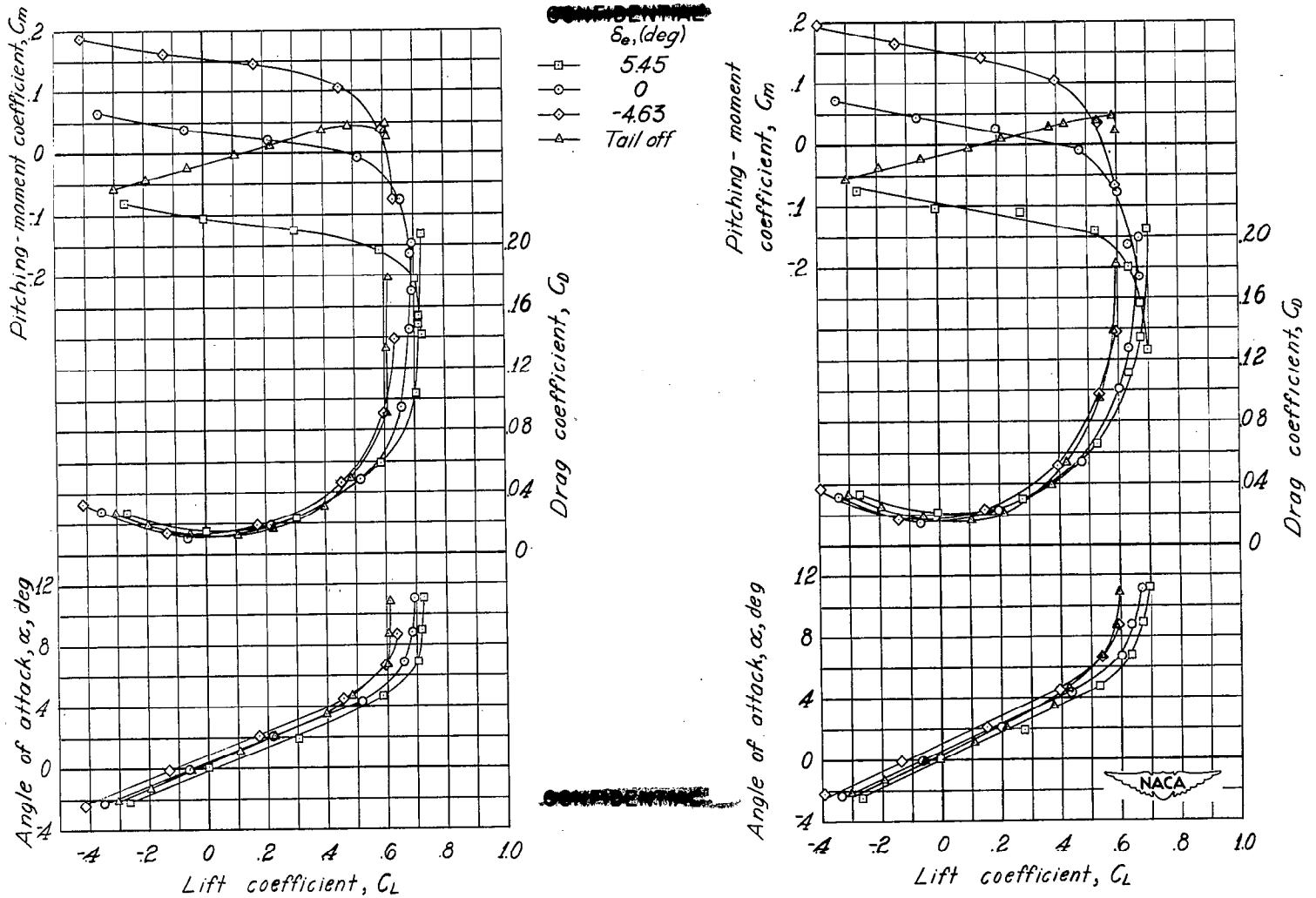

(g) M = 0.775.

(h) M = 0.800.

Figure 8.– Continued.

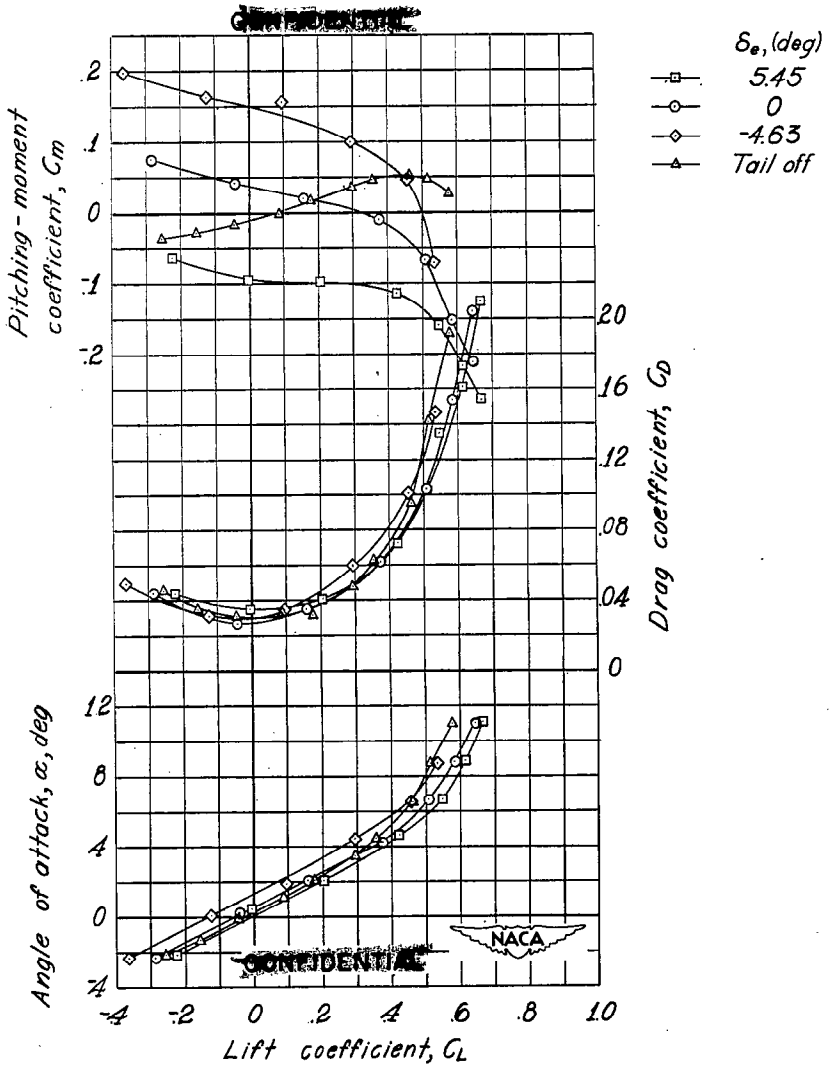

(i) M = 0.825.

Figure 8.– Concluded.

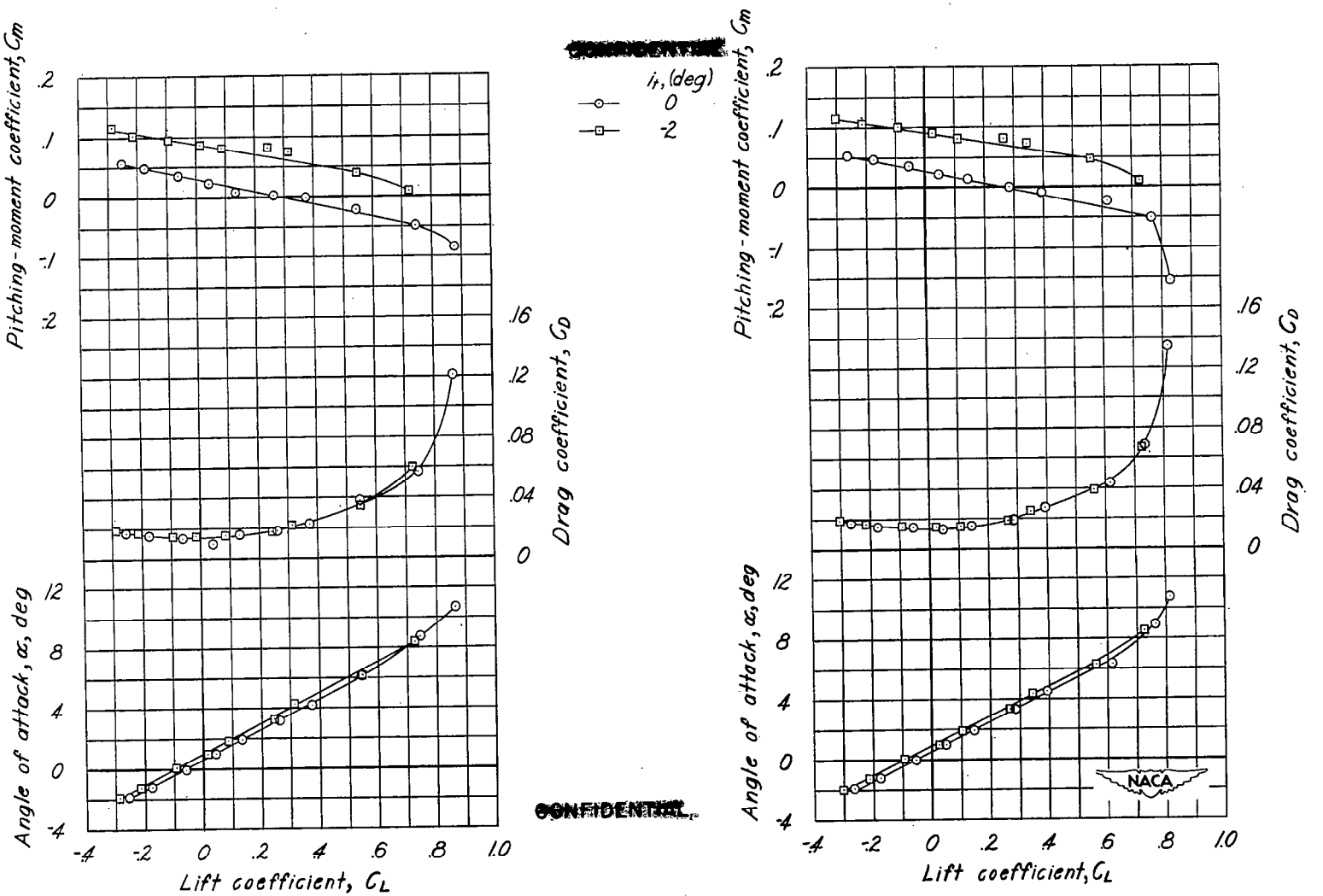

(a) M = 0.400.

(b) M = 0.500.

Figure 9.- Effect of stabilizer setting on the aerodynamic characteristics in pitch of the 0.10-scale model of the XF9F-2 airplane. Plain elevator; tanks on; $\delta_e = 0°$.

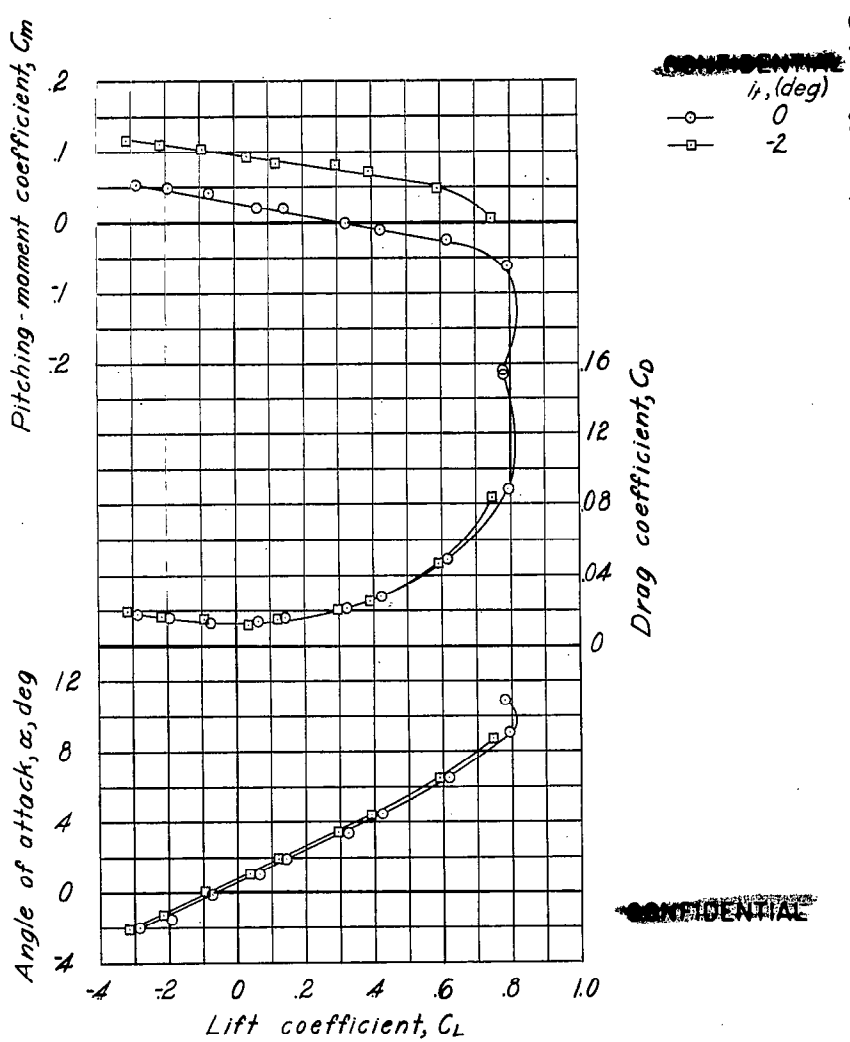

(c) M = 0.600.

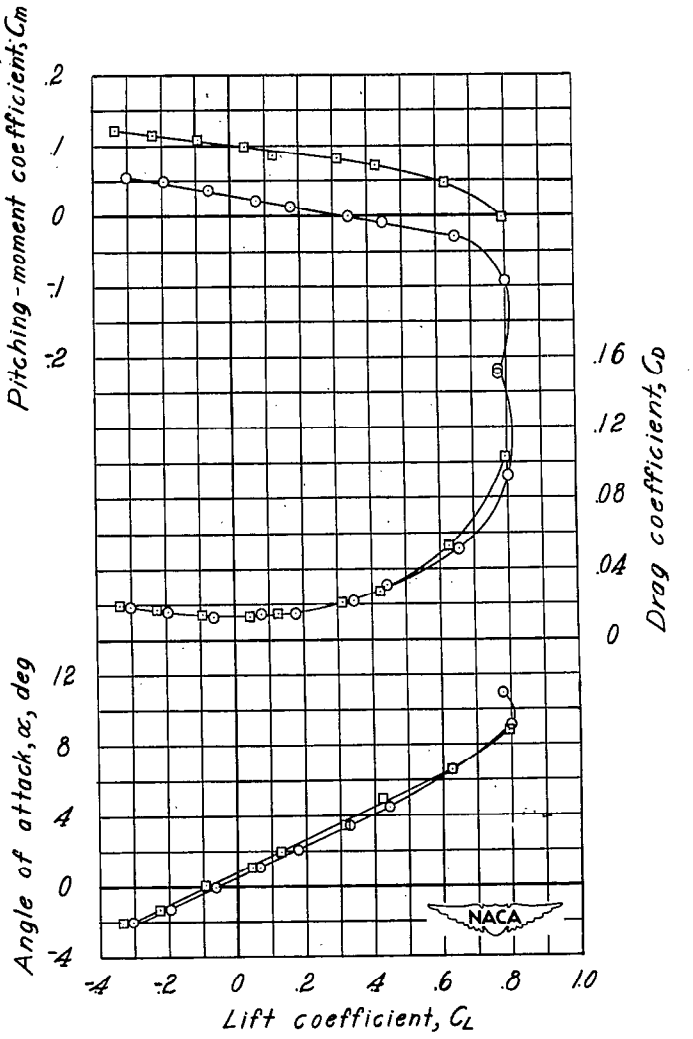

(d) M = 0.650.

Figure 9.- Continued.

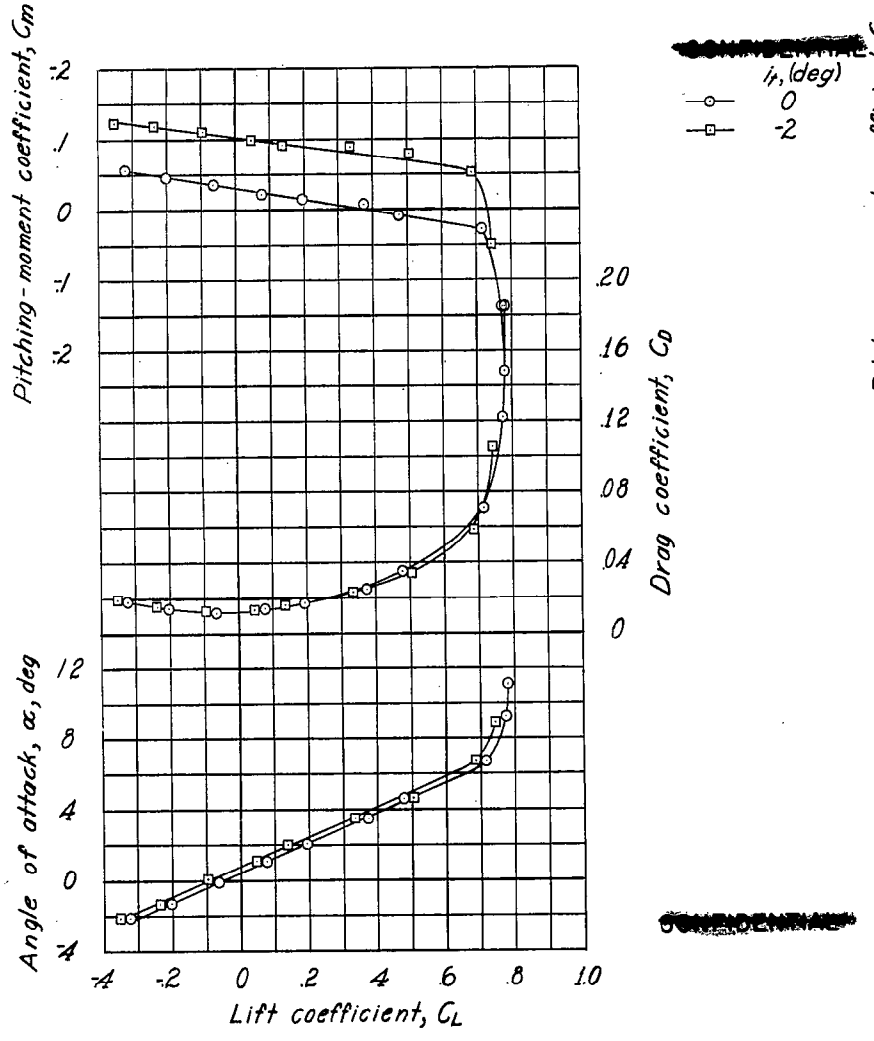

(e) M = 0.700.

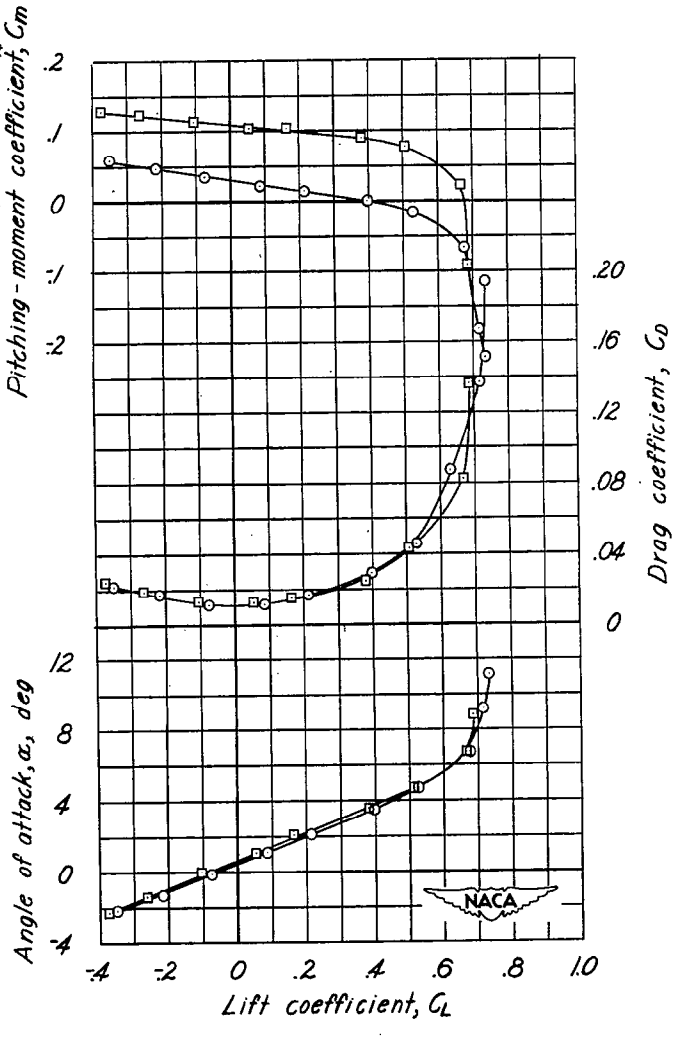

(f) M = 0.750.

Figure 9.– Continued.

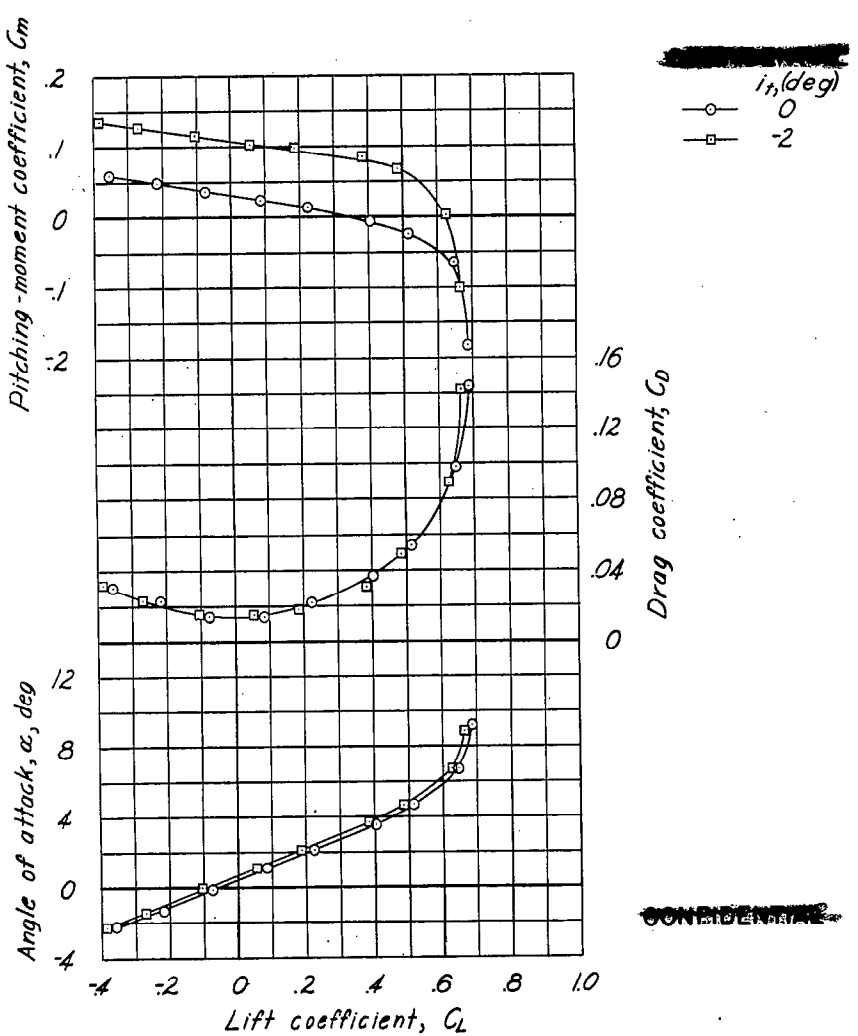

(g) M = 0.775.

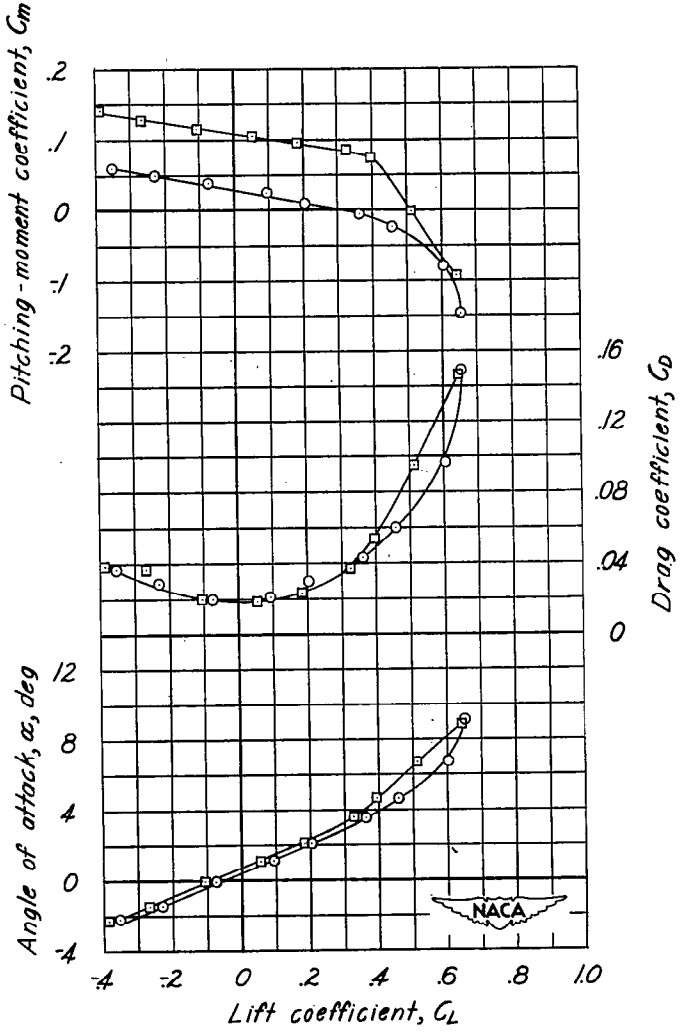

(h) M = 0.800.

Figure 9.– Continued.

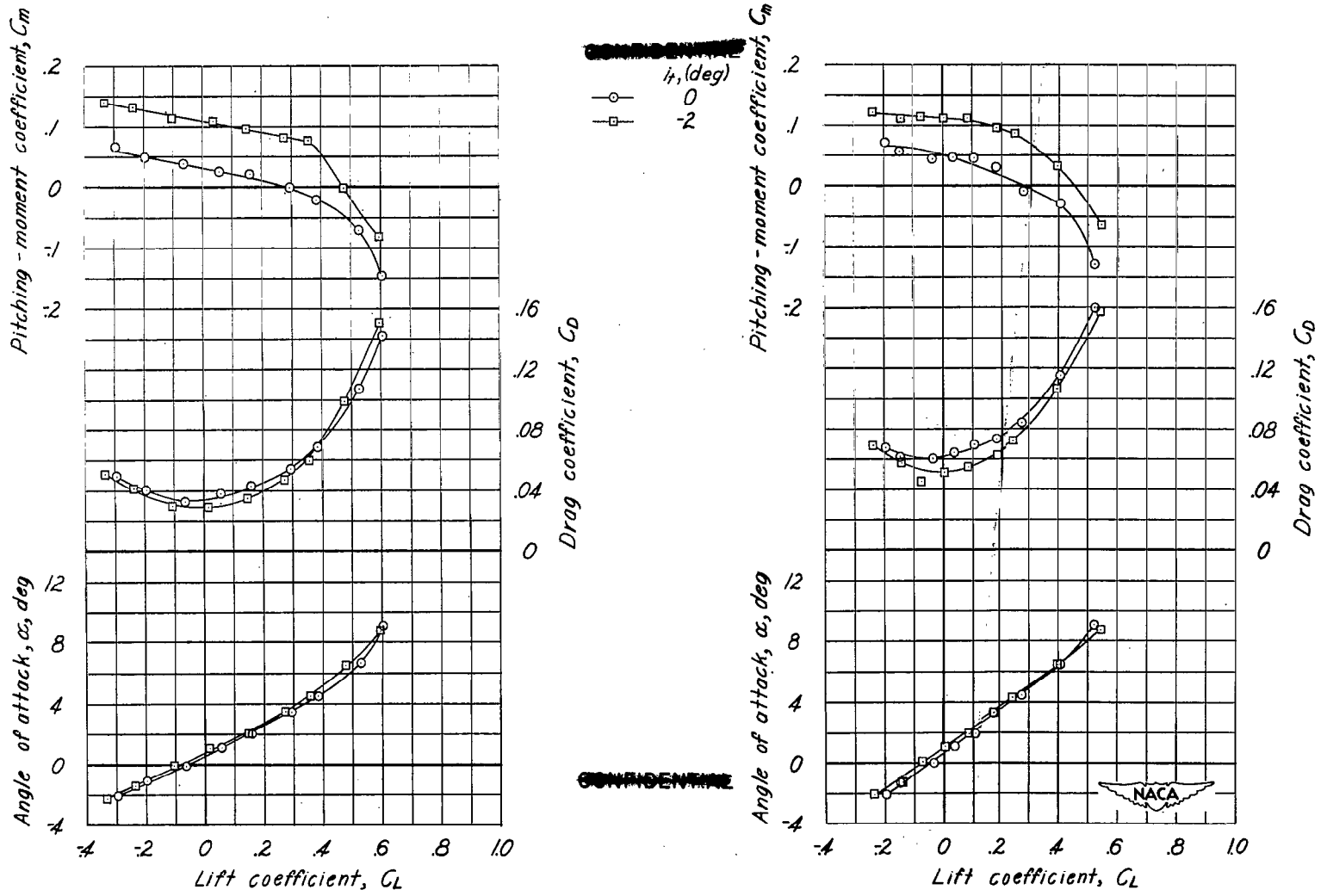

(i) M = 0.825.

(j) M = 0.850.

Figure 9.– Concluded.

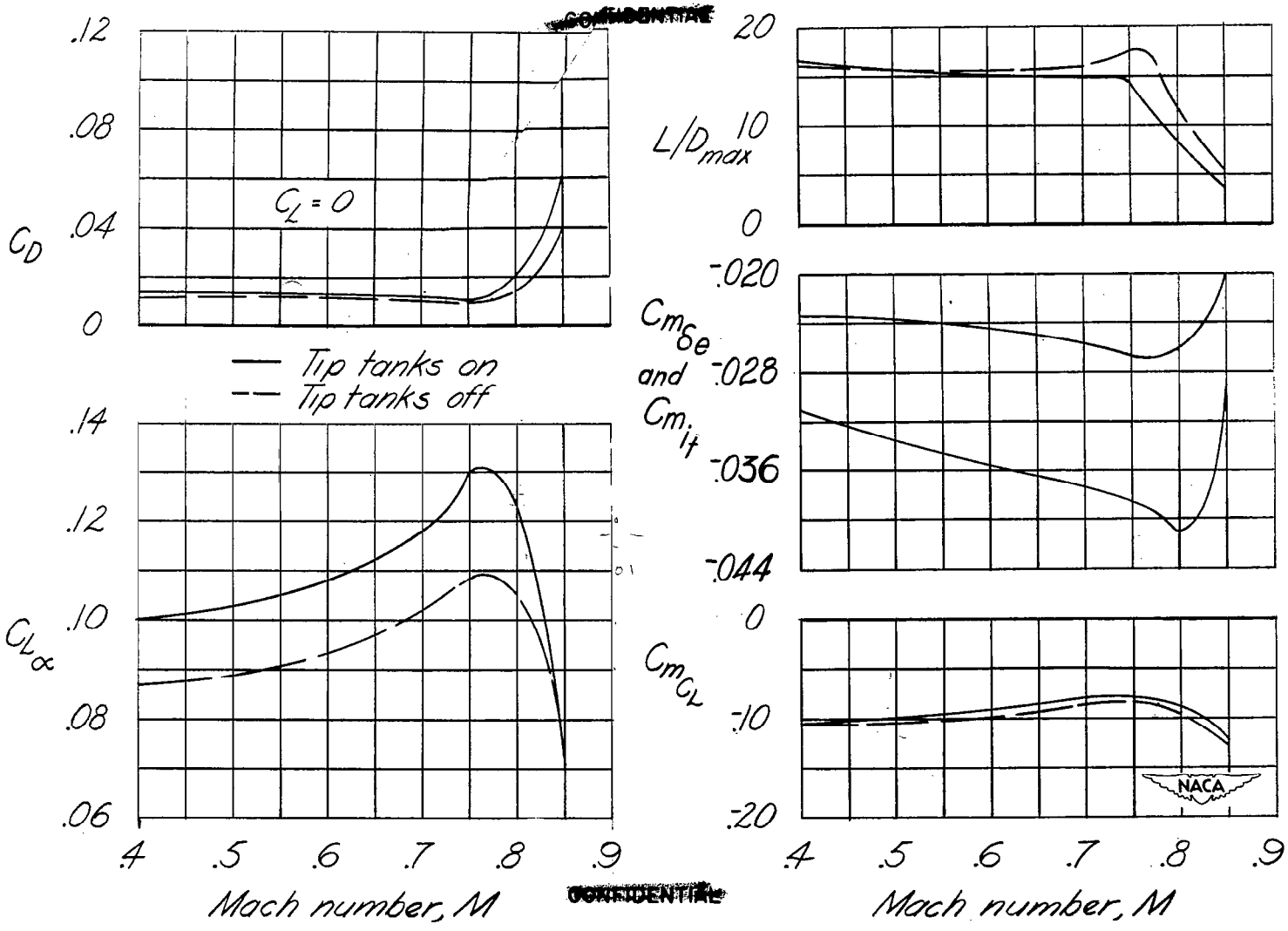

Figure 10.– Effect of Mach number on various aerodynamic characteristics, plain elevator.

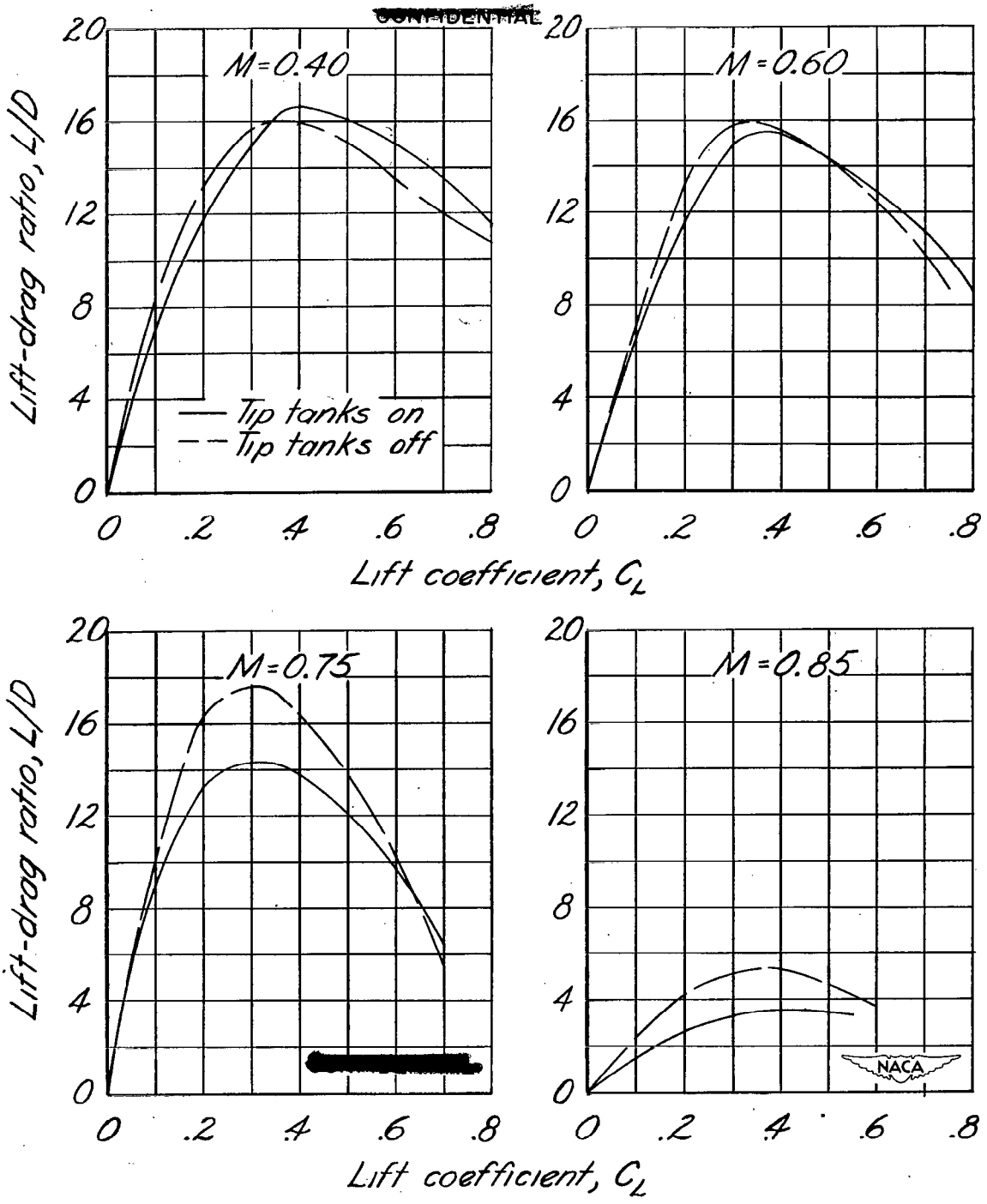

Figure 11.– Effect of wing–tip tanks on the lift–drag ratio of the 0.10–scale model of the XF9F–2 airplane, $i_t = 0^\circ$, plain elevator.

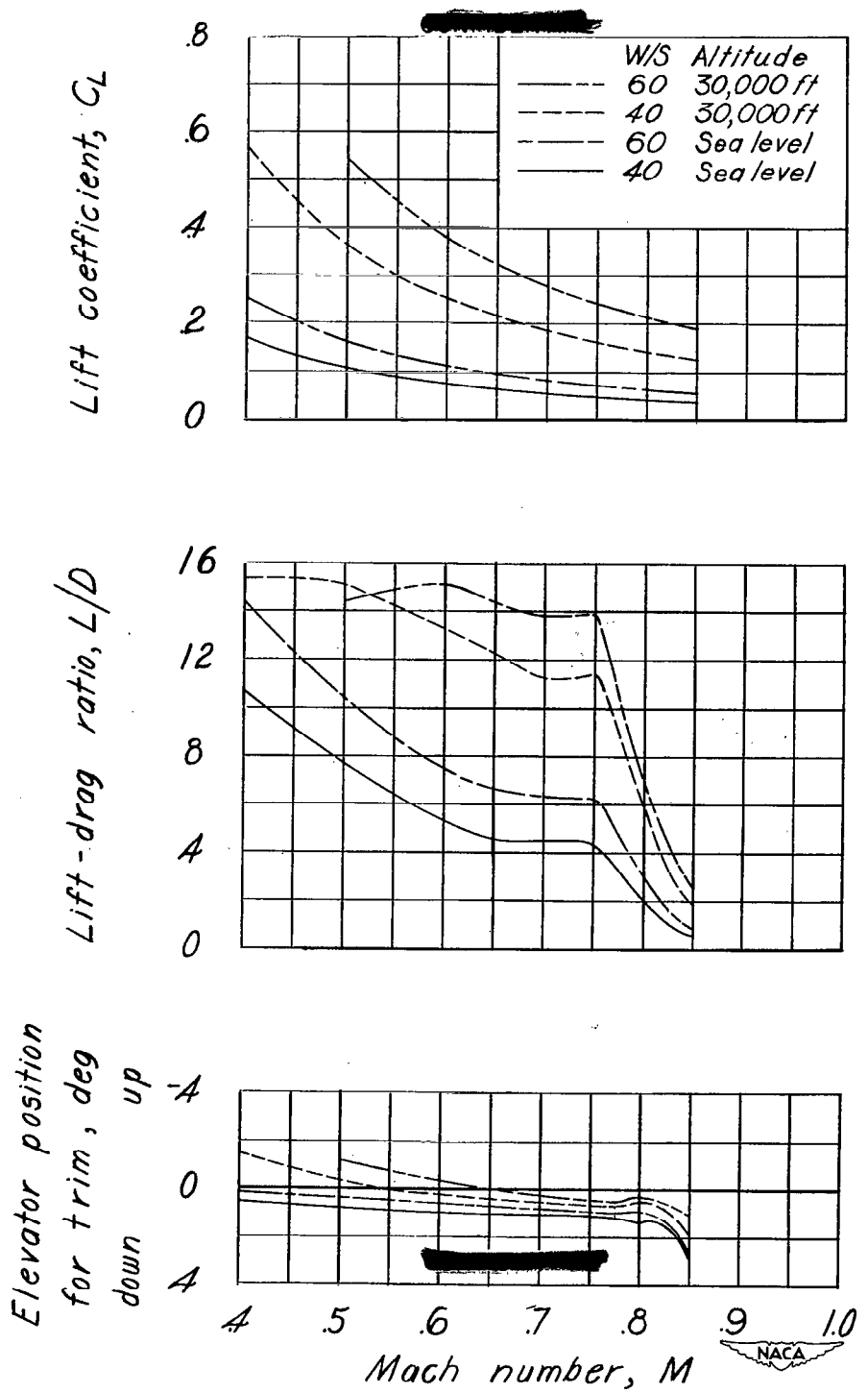

Figure 12.– Variation with Mach number of elevator position and C_L for level flight of the XF9F–2 airplane. Plain elevator; tanks on; $i_t = 0°$. L/D